COMMUN. MATH. SCI.
Vol. 15, No. 1, pp. 1–26
© 2017 International Press

COMPARISON OF SEVERAL REACTION AND DIFFUSION MODELS OF GROWTH FACTORS IN ANGIOGENESIS*

FANG LI† AND XIAOMING ZHENG‡

Abstract. We compare three types of mathematical models of growth factor reaction and diffusion in angiogenesis: one describes the reaction on the blood capillary surface, one on the capillary volume, and one on the capillary centerline. Firstly, we explore the analytical properties of these models, including solution regularity and positivity. We prove that the surface-reaction models have smooth and positive solutions and that the volume-reaction models have continuous and positive solutions. The line-reaction models utilize distributions on the capillary centerline to represent the reaction line source. The line-reaction model-Iemploys the Dirac delta function and the mean value of the growth factor around the centerline, which gives a valid model. The line-reaction model-IIand -IIIuse the local value of the growth factor, which either creates a singularity or decouples the reaction from diffusion, thus being invalid invalid. Secondly, we compare the programming complexity and computational cost of these models in numerical implementations. The surface-reaction model is the most complicated and suitable for small domains, while the volume-reaction and line-reaction models are simpler and suitable for large domains with a large number of blood capillaries. Finally, we quantitatively compare these models in the prediction of the growth factor dynamics. It turns out that the volume-reaction and line-reaction model-Iagree well with the surface-reaction model for most parameters used in the literature but may differ significantly when the diffusion constant is small.

Key words. Reaction, diffusion, angiogenesis, growth factors, equations with distribution coefficients, singular solutions.

AMS subject classifications. 35K57, 36K67, 92B99.

1. Introduction

Angiogenesis, the formation of new blood vessels, is crucial to many processes such as wound healing and cancer. It is controlled by growth factors such as Vascular Endothelial Growth Factor (VEGF). VEGF is released by injured tissue or hypoxic cancer cells and diffuses in the tissue. Once reaching blood vessels, VEGF binds to receptors such as VEGFR2 on endothelial cells that line the blood vessel. The activation of VEGFR2 triggers a sequence of intracellular events resulting in cell proliferation and migration. These new blood vessels are called capillaries because they are very thin. Their radius ranges from 2 to $20\mu m$ [26], but the length can extend to the size of the tissue (for example, $2mm$ in diameter of a rat cornea [26] or a dormant tumor [7]). The reaction (binding kinetics) occurs only on the thin capillaries, while the diffusion happens in the tissue domain.

The purpose of this work is to compare the existing reaction and diffusion models of growth factors in angiogenesis. There exist mainly four types of models, depending on where the binding reaction is modeled. The first type describes the reaction on the capillary surface, such as [5, 13–15, 17]. We call these the surface-reaction models. The second type treats the reaction occurring in the whole capillary volume, such as [3, 6, 10, 16, 19, 28], which is called the volume-reaction model in this paper. The third

*Received: January 13, 2015; accepted (in revised form): May 25, 2015. Communicated by John Lowengrub.
F. Li was partially supported by NSF of China (No. 11431005), NSF of Shanghai (No. 16ZR1409600). Zheng is supported by the Central Michigan University ORSP Early Career Investigator (ECI) grant No. C61373.

†Center for Partial Differential Equations, East China Normal University, Shanghai 200241, P.R. China (fangli0214@gmail.com).
‡Department of Mathematics, Central Michigan University, Mount Pleasant, MI 48859 USA (zheng 1x@cmich.edu). http://people.cst.cmich.edu/zheng1x/

type models the reaction only on the capillary centerline, such as [27, 29, 33], which are called line reaction models. More details of these models will be discussed in Section 2. In the fourth type of models, the endothelial cells and thus the capillaries are defined as densities in the whole tissue domain. Therefore, the binding reactions are defined everywhere in the tissue (for example see [1, 2, 8, 11, 18, 21, 22, 24, 30]). Compared with the first three types of models, the fourth type is less appealing because it smears out the delicate spatial structure of the capillary network. The analysis of the fourth type is simpler and actually contained in the analysis for the volume-reaction models (see Remark 2.2). Therefore, we will only study the first three types of models in this work.

Among all these models, we are most interested in the line-reaction models because of the following reasons. First, geometrically, the thin capillary looks like a zero-thickness curve in a large domain. Therefore, it is tempting to model the reaction on the capillary as a line source. The sources with a Dirac delta function and some given strength have been extensively used in physical and engineering problems. However, the line-reaction models [32, 33] use the unknown solution itself with the Dirac delta function to represent the line source, which is novel in the literature. In addition, there are no rigorous analyses available of these novel models except the work [12] in a reduced case. Therefore, it is of great interest to investigate the analytical features of these full models, such as whether the solution develops singularity.

Although some of these models are popular in the literature, their relations and differences have never been studied. To better illustrate our viewpoints, the comparison will be launched from three aspects: qualitative features, numerical implementations, and quantitative predictions. First, we will study the well-posedness/ill-posedness of each selected model and analyze the qualitative properties of solutions, including regularity and positivity. Next, we will briefly discuss the differences in computational implementations between these models. Finally, we will quantitatively compare one surface-reaction model, one volume-reaction model, and one line-reaction model, the first two of which are popular in existing literature, to find out the parameter regimes where these models agree well.

This paper is organized as follows. The qualitative studies are included in Section 2, which is the main part of this work. The comparison in computer implementations is given in Section 3, while Section 4 is about the comparison in the prediction of growth factor dynamics. Finally, the conclusions are given in Section 5.

2. Comparison in qualitative features

The qualitative features include existence, regularity, and positivity of solutions. In order to determine whether a model is valid or not, we propose the following two criteria:

(C1) Positivity: all the quantities used in reactions must be finite and non-negative.

(C2) Coupling: the reaction and diffusion processes cannot be independent of each other.

The criterion (C1) is very natural because these quantities are reactant concentrations. Note that, as for the growth factor, the quantity used in reactions is not necessarily the local value. For example, in the line-reaction model-Iin Section 2.3, it is the mean value in the capillary volume that is used in reactions. The criterion (C2) prevents the cases where the reaction is rendered completely irrelevant to the diffusion. In reality, the reaction consumes the growth factor molecules delivered by the diffusion process and also releases some of them back to the diffusion. We set the criterion

(C2) because some models seemingly couple these two processes by writing them in the same equation. However, a rigorous analysis indicates that they are actually decoupled (see Section 2.4). A valid model should satisfy both criteria. The main results of the qualitative comparison of several models are briefly summarized in Table 2.1.

Type	Main equations	Full model	Solution u
surface-reaction	$\frac{\partial u}{\partial t} = D\Delta u - \mu u$ in Ω_T, $D\frac{\partial u}{\partial \mathbf{n}} = f_{2d}(u)$ on $\partial\Omega_C$	(2.6)	positive and smooth, Theorem 2.1
volume-reaction	$\frac{\partial u}{\partial t} = D\Delta u - \mu u + \chi_{\Omega_C} f_{3d}(u)$ in Ω	(2.15)	positive and continuous, Theorem 2.2
line-reaction-I	$\frac{\partial u}{\partial t} = D\Delta u - \mu u + \delta_\Sigma f_{3d}(\bar{u})$ in Ω	(2.22)	u has a logrithmic singularity on Σ but $\bar{u}$ is positive, Theorem 2.3 and 2.4
line-reaction-II	$\frac{\partial u}{\partial t} = D\Delta u - \mu u + \chi_\Sigma f_{3d}(u)$ in Ω	(2.37)	invalid, Section 2.4
line-reaction-III	$\frac{\partial u}{\partial t} = D\Delta u - \mu u + \delta_\Sigma f_{3d}(u)$ in Ω	(2.38)	invalid, Theorem 2.5, Section 2.4

TABLE 2.1. *Qualitative comparison of reaction and diffusion models in angiogenesis.*

Consider a domain Ω that contains two disjoint open subdomains: the tissue domain Ω_T and the capillary domain Ω_C, which are shown in Figure 2.1. Denote the boundary between Ω_T and Ω_C as $\partial\Omega_C$, which is the capillary surface. Therefore, $\Omega = \Omega_T \cup \Omega_C \cup \partial\Omega_C$ and $\partial\Omega_T = \partial\Omega \cup \partial\Omega_C$. In this work, we assume that Ω_T and Ω_C are smooth. When multiple capillaries form a complex network through branching and anastomosis, it is still reasonable to assume the Ω_T and Ω_C are smooth, because branching and anastomosis regions can be treated as smooth surfaces. Denote the capillary centerline as Σ. Let r be the radius of the capillary, whose value is between $2 \sim 20\mu m$ [26].

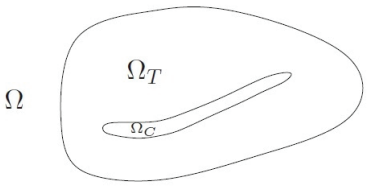

FIG. 2.1. *The tissue domain Ω_T, the capillary domain Ω_C, and the whole domain $\Omega = \Omega_T \cup \Omega_C \cup \partial\Omega_C$.*

2.1. A surface-reaction model. The surface-reaction models study the concentration of receptors on the capillary surface and the concentration of growth factor in the tissue domain. Such models include the VEGF model of Popel's group [5, 13–15] and epidermal growth factor receptor (EGFR) in [17]. A typical model is as follows. Denote u as the volume concentration of the free growth factor in Ω_T, and R_{2d} and C_{2d} as the surface concentrations of free receptors and growth factor/receptor complexes, respectively, on the capillary surface. Therefore, the unit of u is $\frac{mole}{volume}$, while the unit of R_{2d} and C_{2d} is $\frac{mole}{area}$. In general, the governing equations of R_{2d} and C_{2d} are

$$\frac{\partial R_{2d}}{\partial t} = -k_{\text{on}} u R_{2d} + k_{\text{off}} C_{2d} + k_p C_{2d}, \tag{2.1}$$

$$\frac{\partial C_{2d}}{\partial t} = k_{\text{on}} u R_{2d} - k_{\text{off}} C_{2d} - k_p C_{2d}, \tag{2.2}$$

where the constants k_{on}, k_{off}, and k_p are the association rate, the dissociation rate, and the internalization rate, respectively. In this presentation, the diffusion, insertion, and

decay of receptors in the cell are neglected for clarity. The mass transport rate of u from the capillary Ω_C to the tissue Ω_T is

$$f_{2d}(u,\mathbf{P}) \triangleq -k_{\text{on}} u R_{2d} + k_{\text{off}} C_{2d}, \tag{2.3}$$

where $\mathbf{P}$ denotes all other proteins participating, in this reaction and in this case $\mathbf{P} = \{R_{2d}, C_{2d}\}$. The unit of $f_{2d}(u,\mathbf{P})$ is $\frac{mole}{area \cdot time}$. For simplicity, we denote $f_{2d}(u,\mathbf{P})$ as $f_{2d}(u)$ hereafter, and similarly for $f_{3d}(u)$.

Let the Fickian diffusive flux through any surface in Ω_T be $\mathbf{J}_F(u) = -D\nabla u$, where D is the diffusion constant. The growth factor diffuses and decays naturally in the tissue domain, which is modeled by

$$\frac{\partial u}{\partial t} = D\Delta u - \mu u \quad \text{in } \Omega_T, \tag{2.4}$$

where μ is the decay constant. It is a general practice to assume that the normal Fickian flux is equal to the negative growth factor transport rate on the capillary surface, that is,

$$\mathbf{J}_F(u)\cdot\mathbf{n} = -f_{2d}(u) \quad \text{or} \quad D\frac{\partial u}{\partial \mathbf{n}} = f_{2d}(u) \quad \text{on } \partial\Omega_C, \tag{2.5}$$

as in [5, 15, 17]. Here, $\mathbf{n}$ is the unit normal vector on $\partial\Omega_C$ pointing to the interior of Ω_C. Indeed, Equations (2.5) can be rigorously proven (see Appendix A). To close this system, another boundary condition has to be imposed on the outer boundary of Ω_T, $\partial\Omega$, such as the no-flux or Dirichlet condition.

To show the qualitative features of the surface-reaction model, we investigate the following full model:

$$\begin{cases} \frac{\partial u}{\partial t} = D\Delta u - \mu u & \text{for } x \in \Omega_T,\ t>0, \\ \frac{\partial R_{2d}}{\partial t} = -k_{\text{on}} u R_{2d} + k_{\text{off}} C_{2d} + k_p C_{2d} & \text{for } x \in \partial\Omega_C,\ t>0, \\ \frac{\partial C_{2d}}{\partial t} = k_{\text{on}} u R_{2d} - k_{\text{off}} C_{2d} - k_p C_{2d} & \text{for } x \in \partial\Omega_C,\ t>0, \\ D\frac{\partial u}{\partial \mathbf{n}} = -k_{\text{on}} u R_{2d} + k_{\text{off}} C_{2d} & \text{for } x \in \partial\Omega_C,\ t>0, \\ \frac{\partial u}{\partial \mathbf{n}} = 0 & \text{for } x \in \partial\Omega,\ t>0, \end{cases} \tag{2.6}$$

with initial values $u(x,0)$ for $x \in \bar{\Omega}_T$ and $R_{2d}(x,0), C_{2d}(x,0)$ for $x \in \partial\Omega_C$.

Because $\frac{\partial}{\partial t}[R_{2d}(x,t) + C_{2d}(x,t)] = 0$,

$$R_{2d}(x,t) + C_{2d}(x,t) = R_{2d}(x,0) + C_{2d}(x,0) \doteq m(x). \tag{2.7}$$

Note that this model is a coupled system of parabolic and ordinary differential equations with nonlinear boundary conditions studied in [20]. We have the following result.

THEOREM 2.1. *Suppose the domain Ω_T is smooth and the constants $D>0$, $\mu \geq 0$, $k_{on}>0$, $k_{off} \geq 0$, $k_p \geq 0$, and $k_{off}+k_p>0$. Let $u(x,0)$, $R_{2d}(x,0)$, and $C_{2d}(x,0)$ be non-negative smooth functions, $u(x,0) \not\equiv 0$, and $m(x)>0$. There exists a unique solution (u, R_{2d}, C_{2d}) of the model (2.6) which is smooth and positive in $\bar{\Omega}_T \times (0,\infty)$.*

Proof. First, note that the model (2.6) is equivalent to

$$\begin{cases} \frac{\partial u}{\partial t} = D\Delta u - \mu u & \text{for } x \in \Omega_T,\ t>0, \\ \frac{\partial R_{2d}}{\partial t} = -k_{\text{on}} u R_{2d} + k_{\text{off}} C_{2d} + k_p C_{2d} & \text{for } x \in \Omega_T,\ t>0, \\ \frac{\partial C_{2d}}{\partial t} = k_{\text{on}} u R_{2d} - k_{\text{off}} C_{2d} - k_p C_{2d} & \text{for } x \in \Omega_T,\ t>0, \\ D\frac{\partial u}{\partial \mathbf{n}} = -k_{\text{on}} u R_{2d} + k_{\text{off}} C_{2d} & \text{for } x \in \partial\Omega_C,\ t>0, \\ \frac{\partial u}{\partial \mathbf{n}} = 0 & \text{for } x \in \partial\Omega,\ t>0, \\ u(x,0) = u_0(x),\ R_{2d}(x,0) = R_0(x),\ C_{2d}(x,0) = C_0(x) & \text{for } x \in \bar{\Omega}_T, \end{cases} \tag{2.8}$$

where the reaction of R_{2d} and C_{2d} have been extended to the whole domain Ω_T because they do not affect u in $\bar{\Omega}_T$. Using Equation (2.7), the system (2.8) can be reduced to the following equivalent system:

$$\begin{cases} \frac{\partial u}{\partial t} - D\Delta u = -\mu u & \text{for } x \in \Omega_T,\ t>0, \\ \frac{\partial C_{2d}}{\partial t} = k_{\text{on}} u m(x) - (k_{\text{off}} + k_p + k_{\text{on}} u) C_{2d} & \text{for } x \in \Omega_T,\ t>0, \\ D\frac{\partial u}{\partial \mathbf{n}} = -k_{\text{on}} u \cdot (m(x) - C_{2d}) + k_{\text{off}} C_{2d} & \text{for } x \in \partial\Omega_C,\ t>0, \\ \frac{\partial u}{\partial \mathbf{n}} = 0 & \text{for } x \in \partial\Omega,\ t>0, \\ u(x,0) = u_0(x),\ C_{2d}(x,0) = C_0(x) & \text{for } x \in \bar{\Omega}_T. \end{cases} \tag{2.9}$$

We will employ [20, Theorem 3.2] to show the existence and uniqueness of solutions to the system (2.9). To this aim, we will first construct a pair of ordered lower and upper solutions of the system (2.9).

Let $(\underline{u}, \underline{C}_{2d})$ denote the solution to the following linear system:

$$\begin{cases} \frac{\partial \underline{u}}{\partial t} - D\Delta \underline{u} = -\mu \underline{u} & \text{for } x \in \Omega_T,\ t>0, \\ \frac{\partial \underline{C}_{2d}}{\partial t} = -[k_{\text{off}} + k_p + k_{\text{on}} \max_{x\in\Omega_T} u_0(x)] \underline{C}_{2d} & \text{for } x \in \Omega_T,\ t>0, \\ D\frac{\partial \underline{u}}{\partial \mathbf{n}} = -k_{\text{on}} \underline{u} m(x) & \text{for } x \in \partial\Omega_C,\ t>0, \\ \frac{\partial \underline{u}}{\partial \mathbf{n}} = 0 & \text{for } x \in \partial\Omega,\ t>0, \\ \underline{u}(x,0) = u_0(x),\ \underline{C}_{2d}(x,0) = C_0(x) & \text{for } x \in \bar{\Omega}_T. \end{cases} \tag{2.10}$$

For $\underline{u}$, we can apply the maximum principles of parabolic equations (for example see [23, Prop. 52.6 and 52.7] to find that $0 < \underline{u} \le \max_{x\in\Omega_T} u_0(x)$ on $\bar{\Omega}_T \times (0,\infty)$. For $\underline{C}_{2d}$, it is clear that $m(x) \ge \underline{C}_{2d} \ge 0$ on $\bar{\Omega}_T \times (0,\infty)$. Hence, it is easy to verify that $(\underline{u}, \underline{C}_{2d})$ is a lower solution of the system (2.9).

An upper solution can be constructed as follows. Consider

$$\begin{cases} \frac{\partial \tilde{u}}{\partial t} - D\Delta \tilde{u} = -\mu \tilde{u} & \text{for } x \in \Omega_T,\ t>0, \\ \frac{\partial \tilde{C}_{2d}}{\partial t} = 0 & \text{for } x \in \Omega_T,\ t>0, \\ D\frac{\partial \tilde{u}}{\partial \mathbf{n}} = -k_{\text{on}} \tilde{u}(m(x) - \tilde{C}_{2d}) + k_{\text{off}} \tilde{C}_{2d} & \text{for } x \in \partial\Omega_C,\ t>0, \\ \frac{\partial \tilde{u}}{\partial \mathbf{n}} = 0 & \text{for } x \in \partial\Omega,\ t>0, \\ \tilde{u}(x,0) = u_0(x),\ \tilde{C}_{2d}(x,0) = m(x) & \text{for } x \in \bar{\Omega}_T. \end{cases} \tag{2.11}$$

It is easy to see that this system admits a unique solution $(\tilde{u}, \tilde{C}_{2d})$ with $\tilde{C}_{2d}(x,t) \equiv m(x)$ and $\tilde{u} > 0$ on $\bar{\Omega}_T \times (0,\infty)$ by the maximum principles. Similarly, it is easy to check that $(\tilde{u}, \tilde{C}_{2d})$ is an upper solution of the system (2.9).

Moreover, notice that $w \doteq \underline{u} - \tilde{u}$ satisfies

$$\begin{cases} \frac{\partial w}{\partial t} - D\Delta w = -\mu w & \text{for } x \in \Omega_T, t > 0, \\ D\frac{\partial w}{\partial \mathbf{n}} < -k_{\text{on}} m w & \text{for } x \in \partial\Omega_C, t > 0, \\ \frac{\partial w}{\partial \mathbf{n}} = 0 & \text{for } x \in \partial\Omega, t > 0, \\ w(x,0) = 0 & \text{for } x \in \bar{\Omega}_T. \end{cases}$$

Again by the maximum principles, $w = \underline{u} - \tilde{u} < 0$ in $\bar{\Omega}_T \times (0,\infty)$. Therefore, we have obtained a pair of ordered lower and upper solutions of the system (2.9).

Next, denote $S = \{(u, C_{2d}) \in C(\Omega_T) : \underline{u} \le u \le \tilde{u}, \underline{C}_{2d} \le C_{2d} \le \tilde{C}_{2d}\}$. One easily sees that the assumption (H2) in [20, Theorem 3.2] is satisfied. The assumption that Ω_T is smooth satisfies the domain regularity requirement of Theorem 3.2 of [20]. Therefore, the system (2.9) has a unique solution in S, denoted by (u, C_{2d}), which is smooth and non-negative on $\bar{\Omega}_T \times (0,\infty)$. Because $\underline{u}$ is strictly positive, so is u.

Finally, we show the strict positivity of R_{2d} and C_{2d}. In fact, by Equation $(2.9)_2$, it is easy to derive that

$$\begin{aligned} C_{2d}(x,t) = C_0(x) \exp\left(- \int_0^t (k_{\text{on}} u(x,\tau) + k_{\text{off}} + k_p) d\tau \right) \\ + k_{\text{on}} m(x) \int_0^t \exp\left(- \int_\tau^t (k_{\text{on}} u(x,s) + k_{\text{off}} + k_p) ds \right) u(x,\tau) d\tau. \end{aligned}$$

Thus, clearly $C_{2d} > 0$ for $x \in \bar{\Omega}_T$, $t > 0$. Similarly, according to the system (2.6) and Equation (2.7), R_{2d} can be solved to obtain that

$$\begin{aligned} R_{2d}(x,t) = R_0(x) \exp\left(- \int_0^t (k_{\text{on}} u(x,\tau) + k_{\text{off}} + k_p) d\tau \right) \\ + (k_{\text{off}} + k_p) m(x) \int_0^t \exp\left(- \int_\tau^t (k_{\text{on}} u(x,s) + k_{\text{off}} + k_p) ds \right) d\tau. \end{aligned}$$

Hence, it follows that $R_{2d} > 0$ for $x \in \bar{\Omega}_T$, $t > 0$. ∎

2.2. A volume-reaction model. In the surface-reaction models, the free receptors and complexes are surface concentrations defined on the capillary surface $\partial\Omega_C$. However, in the volume-reaction models, the free receptors and complexes become volume concentrations defined in the volume Ω_C. Therefore, it is helpful to derive a relation between the surface and volume concentrations of these quantities in order to better understand the relations between these two types of models.

One way to connect the surface concentration g_{2d} (representing R_{2d}, C_{2d}, etc.) of some quantity to its volume concentration g_{3d} (say, R_{3d}, C_{3d}, etc.) is based on the mass conservation. On a cross-section of the capillary volume with radius r, we that assume the concentration is a constant on it. The mass conservation implies $g_{3d}\pi r^2 = g_{2d} 2\pi r$, which leads to

$$g_{3d} = \frac{2}{r} g_{2d}. \tag{2.12}$$

Therefore, the area transfer rate f_{2d} can be converted to the volume transfer rate as

$$f_{3d} = \frac{2}{r} f_{2d} = \frac{2}{r}(-k_{\text{on}} u R_{2d} + k_{\text{off}} C_{2d}) = -k_{\text{on}} u R_{3d} + k_{\text{off}} C_{3d}. \tag{2.13}$$

In the volume-reaction models, the growth factor equation is typically written as

$$\frac{\partial u}{\partial t} = D\Delta u - \mu u + \chi_{\Omega_C} f_{3d}(u) \quad \text{in } \Omega, \tag{2.14}$$

where χ_{Ω_C} is the characteristic function of the capillary cylinder, which is 1 in the capillary volume and 0 otherwise. This equation has been used in [3, 6, 10, 16, 19, 28]. However, receptors are lacking in these models except in [6]. Indeed, the receptor equations of R_{3d} and C_{3d} can be derived by simply replacing R_{2d} by R_{3d} and C_{2d} by C_{3d} in Equations (2.1) and (2.2). Hence, a full volume-reaction model can be written as follows:

$$\begin{cases} \frac{\partial u}{\partial t} = D\Delta u - \mu u + \chi_{\Omega_C}(-k_{\text{on}} u R_{3d} + k_{\text{off}} C_{3d}) & \text{for } x \in \Omega,\ t > 0, \\ \frac{\partial R_{3d}}{\partial t} = -k_{\text{on}} u R_{3d} + k_{\text{off}} C_{3d} + k_p C_{3d} & \text{for } x \in \Omega_C,\ t > 0, \\ \frac{\partial C_{3d}}{\partial t} = k_{\text{on}} u R_{3d} - k_{\text{off}} C_{3d} - k_p C_{3d} & \text{for } x \in \Omega_C,\ t > 0, \\ \frac{\partial u}{\partial \mathbf{n}} = 0 & \text{for } x \in \partial\Omega,\ t > 0, \\ u(x,0), R_{3d}(x,0), C_{3d}(x,0) \text{ are smooth,} \end{cases} \tag{2.15}$$

where Ω is a smooth bounded domain in $\mathbb{R}^3$ and $\mathbf{n}$ is the unit outward normal vector on $\partial\Omega$. Notice that $\frac{\partial}{\partial t}[R_{3d}(x,t) + C_{3d}(x,t)] = 0$. Thus,

$$R_{3d}(x,t) + C_{3d}(x,t) = R_{3d}(x,0) + C_{3d}(x,0) \doteq m(x). \tag{2.16}$$

Here we have abused the use of symbol $m(x)$ compared with Equation (2.7), where they differ by a constant multiplication factor.

For convenience, let us recall the definition of the Banach space $W_p^{2,1}(\Omega \times (0,T))$, $1 \le p \le \infty$ here. For $u \in L^p(\Omega \times (0,T))$, define

$$\|u\|_{W_p^{2,1}(\Omega\times(0,T))} = \left(\sum_{0 \le r+2s \le 2} \|D_t^s D_x^r u\|^p_{L^p(\Omega\times(0,T))} \right)^{1/p}.$$

We say $u \in W_p^{2,1}(\Omega \times (0,T))$ if $\|u\|_{W_p^{2,1}(\Omega\times(0,T))} < \infty$.

THEOREM 2.2. *Suppose the domain Ω is smooth and the constants $D > 0$, $\mu \ge 0$, $k_{on} > 0$, $k_{off} \ge 0$, $k_p \ge 0$, and $k_{off} + k_p > 0$. Let $u(x,0)$, $R_{3d}(x,0)$, and $C_{3d}(x,0)$ be non-negative smooth functions, $u(x,0) \not\equiv 0$ and $R_{3d}(x,0) + C_{3d}(x,0) > 0$. Then the solution $u(x,t)$ of the system (2.15) belongs to $W_p^{2,1}(\Omega \times (0,T))$, where $p > 1$ and $T > 0$, and u, R_{3d}, and C_{3d} are positive at any time $t > 0$.*

Proof. As in the proof of Theorem 2.1, the reactions of R_{3d} and C_{3d} can be extended to the whole domain Ω, and R_{3d} can be eliminated. Hence, the system (2.15) can be reduced to the following equivalent system:

$$\begin{cases} \frac{\partial u}{\partial t} - D\Delta u = -\mu u + \chi_{\Omega_C}(-k_{\text{on}} u \cdot (m(x) - C_{3d}) + k_{\text{off}} C_{3d}) & \text{for } x \in \Omega,\ t > 0, \\ \frac{\partial C_{3d}}{\partial t} = k_{\text{on}} u m(x) - (k_{\text{off}} + k_p + k_{\text{on}} u) C_{3d} & \text{for } x \in \Omega,\ t > 0, \\ D\frac{\partial u}{\partial \mathbf{n}} = 0 & \text{for } x \in \partial\Omega,\ t > 0. \end{cases} \tag{2.17}$$

Next for any fixed $p > 1$, we replace χ_{Ω_C} with a smooth function $\chi^\epsilon_{\Omega_C} \ge 0$, which converges to χ_{Ω_C} in $L^p(\Omega)$ as $\epsilon \to 0$. Then we obtain

$$\begin{cases} \frac{\partial u^\epsilon}{\partial t} - D\Delta u^\epsilon = -\mu u^\epsilon + \chi^\epsilon_{\Omega_C}(-k_{\text{on}} u^\epsilon \cdot (m(x) - C^\epsilon_{3d}) + k_{\text{off}} C^\epsilon_{3d}) & \text{for } x \in \Omega,\ t > 0, \\ \frac{\partial C^\epsilon_{3d}}{\partial t} = k_{\text{on}} u^\epsilon m(x) - (k_{\text{off}} + k_p + k_{\text{on}} u^\epsilon) C^\epsilon_{3d} & \text{for } x \in \Omega,\ t > 0, \\ D\frac{\partial u}{\partial \mathbf{n}} = 0 & \text{for } x \in \partial\Omega,\ t > 0. \end{cases} \tag{2.18}$$

We will find a solution $(u^\epsilon, C^\epsilon_{3d})$ of the system (2.18) and then let $\epsilon \to 0$ to obtain the solution of the system (2.17).

Similar to Theorem 2.1, the lower solution $(\underline{u}^\epsilon, \underline{C}^\epsilon_{2d})$ can be constructed from the following linear system:

$$\begin{cases} \frac{\partial \underline{u}^\epsilon}{\partial t} - D\Delta \underline{u}^\epsilon = -\mu \underline{u}^\epsilon + \chi^\epsilon_{\Omega_C}(-k_{\text{on}}\underline{u}^\epsilon \cdot m(x)) & \text{for } x \in \Omega,\, t>0, \\ \frac{\partial \underline{C}^\epsilon_{3d}}{\partial t} = -(k_{\text{off}} + k_p + k_{\text{on}} \max_{x\in\Omega} u_0(x)) \underline{C}^\epsilon_{3d} & \text{for } x \in \Omega,\, t>0, \\ \frac{\partial \underline{u}}{\partial \mathbf{n}} = 0 & \text{for } x \in \partial\Omega,\, t>0, \\ \underline{u}^\epsilon(x,0) = u(x,0),\ \underline{C}^\epsilon_{3d}(x,0) = C_{3d}(x,0) & \text{for } x \in \Omega. \end{cases}$$

Also, the upper solution $(\tilde{u}^\epsilon, \tilde{C}^\epsilon_{3d})$ can be constructed from the following system:

$$\begin{cases} \frac{\partial \tilde{u}^\epsilon}{\partial t} - D\Delta \tilde{u}^\epsilon = -\mu \tilde{u}^\epsilon + \chi^\epsilon_{\Omega_C}(-k_{\text{on}}\tilde{u}^\epsilon \cdot (m(x) - \tilde{C}^\epsilon_{3d}) + k_{\text{off}}\tilde{C}^\epsilon_{3d}) & \text{for } x \in \Omega,\, t>0, \\ \frac{\partial \tilde{C}^\epsilon_{3d}}{\partial t} = 0 & \text{for } x \in \Omega,\, t>0, \\ \frac{\partial \tilde{u}^\epsilon}{\partial \mathbf{n}} = 0 & \text{for } x \in \partial\Omega,\, t>0, \\ \tilde{u}^\epsilon(x,0) = u(x,0),\ \tilde{C}^\epsilon_{3d}(x,0) = m(x) & \text{for } x \in \Omega. \end{cases}$$

Therefore, the system (2.18) has a unique positive classical solution $(u^\epsilon, C^\epsilon_{3d})$ in $\bar{\Omega} \times (0,\infty)$ for any $\epsilon > 0$.

Let $\epsilon \to 0$. Then, it is routine to check that, by passing to a subsequence if necessary, the sequence $(u^\epsilon, C^\epsilon_{3d})$ converges to the unique weak solution of the system (2.17). Then by parabolic regularity, we obtain that for any $p>1$, $u(x,t) \in W^{2,1}_p(\Omega \times (0,T))$ for any $T>0$. Moreover, the positivity of $u(x,t)$ follows easily from the strong maximum principle. Similar to the proof of Theorem 2.1, we can prove that R_{3d} and C_{3d} are strictly positive for any $t>0$. ∎

REMARK 2.1. The regularity of the solution $u(x,t)$ in Theorem 2.2 is optimal because of the characteristic function χ_{Ω_C} in the system (2.17). Moreover, according to the parabolic embedding theorem, the solution $u(x,t)$ is C^1 continuous in x and continuous in t.

REMARK 2.2. In the fourth type of models mentioned in Section 1, the blood vessel capillaries are represented as a smooth density function, $\rho(x)$, defined in the whole domain. Its model can be written as

$$\begin{cases} \frac{\partial u}{\partial t} = D\Delta u - \mu u + \rho(-k_{\text{on}} u R_{3d} + k_{\text{off}} C_{3d}) & \text{for } x \in \Omega,\, t>0, \\ \frac{\partial R_{3d}}{\partial t} = -k_{\text{on}} u R_{3d} + k_{\text{off}} C_{3d} + k_p C_{3d} & \text{for } x \in \Omega,\, t>0, \\ \frac{\partial C_{3d}}{\partial t} = k_{\text{on}} u R_{3d} - k_{\text{off}} C_{3d} - k_p C_{3d} & \text{for } x \in \Omega,\, t>0, \\ \frac{\partial u}{\partial \mathbf{n}} = 0 & \text{for } x \in \partial\Omega,\, t>0, \end{cases}$$

where the initial values $u(x,0), R_{3d}(x,0), C_{3d}(x,0)$ are smooth. Applying the analysis for the system (2.18), we obtain that the above system has a smooth and positive solution (u, R_{3d}, C_{3d}).

2.3. Line-reaction model-I. Zheng et al. [32] proposed a model with the reactions on the capillary centerline,

$$\frac{\partial u}{\partial t} = D\Delta u - \mu u + \delta_\Sigma f_{3d}(\bar{u}). \tag{2.19}$$

We call this line-reaction model-I. In this model, $\bar{u}$ is the mean value of u in a cross-section of the capillary. The distribution coefficient δ_Σ is the line Dirac delta function

associated with a smooth one-dimensional curve $\Sigma=\gamma(\ell)$, $\ell\in[0,1]$, which is defined as follows. For any test function $\phi(x)\in\mathcal{S}(\mathbb{R}^3)$ (the Schwartz space or space of rapidly decreasing functions),

$$\int_{\mathbb{R}^3}\delta_\Sigma(x)\phi(x)dx=\int_0^1|C(s)||\gamma'(s)|\phi(\gamma(s))ds, \tag{2.20}$$

where $C(s)$ is the area of the capillary cross-section at $\gamma(s)$. If the radius of the blood vessel capillary is a constant of value r, then $C(s)=\pi r^2$. In [32], the receptor equations for R_{3d} and C_{3d} on Σ are

$$\frac{\partial R_{3d}}{\partial t}=-k_{\rm on}\bar{u}R_{3d}+k_{\rm off}C_{3d}+k_pC_{3d},\quad \frac{\partial C_{3d}}{\partial t}=k_{\rm on}\bar{u}R_{3d}-k_{\rm off}C_{3d}-k_pC_{3d}. \tag{2.21}$$

For simplicity, we consider a cross-section of the capillary in the infinitely large tissue plane $\mathbb{R}^2$ and assume the center of the capillary is at $x=0$. For any function $g(x)$ defined on this plane, we denote its mean value in the capillary as

$$\bar{g}=\frac{1}{\pi r^2}\int_{B_r(0)}g(x)dx,$$

where $B_r(0)=\{x\in\mathbb{R}^2:|x|<r\}$. In this case, this model can be written as

$$\begin{cases}\frac{\partial u}{\partial t}=D\Delta u-\mu u+\pi r^2\delta^{2D}(x)(-k_{\rm on}\bar{u}R_{3d}+k_{\rm off}C_{3d}) & \text{for } x\in\mathbb{R}^2,\ t>0,\\ \frac{dR_{3d}}{dt}=-k_{\rm on}\bar{u}R_{3d}+k_{\rm off}C_{3d}+k_pC_{3d} & \text{for } t>0,\\ \frac{dC_{3d}}{dt}=k_{\rm on}\bar{u}R_{3d}-k_{\rm off}C_{3d}-k_pC_{3d} & \text{for } t>0,\\ u(x,0)=u_0(x)\geq 0,\ R_{3d}(0)=R_0>0,\ C_{3d}(0)=C_0>0,\end{cases} \tag{2.22}$$

where R_0 and C_0 are constants. Note that both R_{3d} and C_{3d} are only defined at $x=0$. Thus, their notations become $R_{3d}=R_{3d}(t)$ and $C_{3d}=C_{3d}(t)$.

REMARK 2.3. A simplified version of the system (2.22) has been analyzed in [12]: when $(-k_{\rm on}\bar{u}R_{3d}+k_{\rm off}C_{3d})$ is replaced with the Michaelis–Menten kinetics:

$$\frac{\partial u}{\partial t}=D\Delta u-\mu u+\delta^{2D}(x)K(\bar{u})\quad\text{in }\mathbb{R}^2,$$

where $K(\bar{u})=-\pi r^2\frac{k_{max}\bar{u}}{k_n+\bar{u}}$, $k_{max}=k_pR_T$, $k_n=\frac{k_{\rm off}+k_p}{k_{\rm on}}$.

THEOREM 2.3. *Assume that D, R_0, and C_0 are positive constants and $u_0(x)\in L^\infty(\mathbb{R}^2)\bigcap C(\mathbb{R}^2)$ is non-negative with $\bar{u}_0>0$. Then, the system (2.22) admits a unique solution when $t>0$ is small. Moreover, $u(x,t)$ is locally integrable and analytic in $\mathbb{R}^2\setminus\{0\}$. In fact, $u(x,t)$ satisfies*

$$\begin{aligned}u(x,t)=&\frac{e^{-\mu t}}{4D\pi t}\int_{\mathbb{R}^2}\exp\left(-\frac{|x-y|^2}{4Dt}\right)u_0(y)dy\\&+r^2\int_0^t\frac{e^{-\mu(t-\tau)}}{4D(t-\tau)}\exp\left(-\frac{|x|^2}{4D(t-\tau)}\right)(-k_{on}\bar{u}(\tau)R_{3d}(\tau)+k_{off}C_{3d}(\tau))d\tau,\end{aligned} \tag{2.23}$$

where $\bar{u}$ is a positive continuous function satisfying

$$\bar{u}(t)=\frac{e^{-\mu t}}{4D\pi t}\frac{1}{\pi r^2}\int_{B_r(0)}\int_{\mathbb{R}^2}\exp\left(-\frac{|x-y|^2}{4Dt}\right)u_0(y)dydx$$

$$+\int_0^t \left[1-\exp\left(-\frac{r^2}{4D(t-\tau)}\right)\right] e^{-\mu(t-\tau)}(-k_{on}\bar{u}(\tau)R_{3d}(\tau)+k_{off}C_{3d}(\tau))d\tau. \quad (2.24)$$

Proof. The main idea is to employ the Banach fixed point theorem. To this aim, some preliminary calculations will be prepared first.

Assume that $h(t)$ is a positive continuous function with $h(0)=\bar{u}_0>0$. Let $(R_h(t),C_h(t))$ denote the solution of the following system of ODEs:

$$\begin{cases} \frac{dR_h}{dt} = -k_{\rm on}h(t)R_h + k_{\rm off}C_h + k_pC_h & \text{for } t>0, \\ \frac{dC_h}{dt} = k_{\rm on}h(t)R_h - k_{\rm off}C_h - k_pC_h & \text{for } t>0, \\ R_h(0)=R_0>0, \quad C_h(0)=C_0>0. \end{cases} \quad (2.25)$$

Then, it will be shown that the solution $(R_h(t),C_h(t))$ can be expressed explicitly.

Notice that

$$\frac{d}{dt}(R_h+C_h)=0.$$

Thus, $R_h(t)+C_h(t)=R_0+C_0\doteq M$, which gives $R_h(t)$ satisfying

$$\begin{cases} \frac{dR_h}{dt} = (k_{\rm off}+k_p)M - (k_{\rm on}h(t)+k_{\rm off}+k_p)R_h & \text{for } t>0, \\ R_h(0)=R_0>0. \end{cases}$$

It is standard to derive that

$$\begin{aligned} R_h(t) = R_0\exp\left(-\int_0^t (k_{\rm on}h(\tau)+k_{\rm off}+k_p)d\tau\right) \\ +(k_{\rm off}+k_p)M\int_0^t \exp\left(-\int_\tau^t (k_{\rm on}h(s)+k_{\rm off}+k_p)ds\right)d\tau. \end{aligned} \quad (2.26)$$

Similarly, $C_h(t)$ can be expressed explicitly as

$$\begin{aligned} C_h(t) = C_0\exp\left(-\int_0^t (k_{\rm on}h(\tau)+k_{\rm off}+k_p)d\tau\right) \\ +k_{\rm on}M\int_0^t \exp\left(-\int_\tau^t (k_{\rm on}h(s)+k_{\rm off}+k_p)ds\right)h(\tau)d\tau. \end{aligned} \quad (2.27)$$

Note that Equations (2.26) and (2.27) clearly indicate that

$$0<R_h(t),\ C_h(t)<M, \quad \text{for } t>0. \quad (2.28)$$

Next, denote

$$K_h(t) = -k_{\rm on}h(t)R_h + k_{\rm off}C_h$$

and consider the following problem:

$$\begin{cases} \frac{\partial u}{\partial t} = D\Delta u - \mu u + \pi r^2\delta^{2D}(x)K_h(t) & \text{for } x\in\mathbb{R}^2,\ t>0, \\ u(x,0)=u_0 & \text{for } x\in\mathbb{R}^2. \end{cases} \quad (2.29)$$

Similar to the computation in [12], by the Fourier transform, we derive that

$$u(x,t) = \frac{e^{-\mu t}}{4D\pi t}\int_{\mathbb{R}^2}\exp\left(-\frac{|x-y|^2}{4Dt}\right)u_0(y)dy$$

$$+r^2\int_0^t \frac{e^{-\mu(t-\tau)}}{4D(t-\tau)}\exp\left(-\frac{|x|^2}{4D(t-\tau)}\right)K_h(\tau)d\tau.$$

For simplicity, we denote

$$I(x,t)=\frac{1}{4D\pi t}\int_{\mathbb{R}^2}\exp\left(-\frac{|x-y|^2}{4Dt}\right)u_0(y)dy.$$

Direct calculation yields that

$$\begin{aligned}\bar{u}(t)&=\frac{1}{\pi r^2}\int_{B_r(0)}u(x,t)dx\\&=e^{-\mu t}\bar{I}(t)+\frac{1}{\pi}\int_{B_r(0)}\int_0^t\frac{e^{-\mu(t-\tau)}}{4D(t-\tau)}\exp\left(-\frac{|x|^2}{4D(t-\tau)}\right)K_h(\tau)d\tau dx\\&=e^{-\mu t}\bar{I}(t)+\int_0^t\left[1-\exp\left(-\frac{r^2}{4D(t-\tau)}\right)\right]e^{-\mu(t-\tau)}K_h(\tau)d\tau.\end{aligned}\tag{2.30}$$

Now, we are ready to define the following mapping

$$(\mathcal{F}h)(t)=e^{-\mu t}\bar{I}(t)+\int_0^t\left[1-\exp\left(-\frac{r^2}{4D(t-\tau)}\right)\right]e^{-\mu(t-\tau)}K_h(\tau)d\tau.\tag{2.31}$$

To show the local solvability of the problem (2.22), it suffices to show that the mapping $\mathcal{F}$ has a fixed point in some suitable set of positive continuous functions in small time intervals.

To be more specific, denote

$$\mathcal{S}_C=\{h(t)\in C([0,\infty))\mid h(0)=\bar{u}_0>0,\ 0<h\le C\}$$

and

$$\mathcal{S}_C^T=\{h(t)\in C([0,T])\mid h(0)=\bar{u}_0>0,\ \bar{u}_0/2\le h\le C\}.$$

Then, in order to apply the Banach fixed point theorem, we will demonstrate that, for certain positive constants C and T, we have the following:

(A) $\mathcal{F}$ maps $\mathcal{S}_C^T$ into itself;

(B) $\mathcal{F}$ is a contraction mapping.

The choice of C and T will be designated later.

Proof. (Proof of (A).) It suffices to show that there exits $t_1>0$ small enough such that $\mathcal{F}$ maps $\mathcal{S}_C^{t_1}$ into itself, where $C\doteq 2\bar{u}_0+M$.

First, since $u_0\in L^\infty(\mathbb{R}^2)\bigcap C(\mathbb{R}^2)$, one sees that $\bar{I}(t)$ is continuous in t. Thus, there exists t_0 such that $3\bar{u}_0/4<\bar{I}(t)<2\bar{u}_0$ for $0<t<t_0$.

Now, on the one hand, we show that, for any positive continuous function $h(t)$,

$$(\mathcal{F}h)(t)<2\bar{u}_0e^{-\mu t}+M\quad\text{for } 0<t<t_0.$$

Notice that

$$K_h(t)=\frac{dR_h}{dt}-k_pC_h.$$

Then, by Equations (2.28) and (2.31), it is straightforward to check that

$$\begin{aligned}(\mathcal{F}h)(t) &= e^{-\mu t}\bar{I}(t)+\int_0^t\left[1-\exp\left(-\frac{r^2}{4D(t-\tau)}\right)\right]e^{-\mu(t-\tau)}\left(\frac{dR_h}{d\tau}-k_pC_h\right)d\tau\\ &< e^{-\mu t}\bar{I}(t)+R_h(t)-\left[1-\exp\left(-\frac{r^2}{4Dt}\right)\right]e^{-\mu t}R_h(0)\\ &\quad-\int_0^t R_h(\tau)\left[1-\exp\left(-\frac{r^2}{4D(t-\tau)}\right)\right]\mu e^{-\mu(t-\tau)}d\tau\\ &\quad-\int_0^t R_h(\tau)\frac{r^2}{4D(t-\tau)^2}\exp\left(-\frac{r^2}{4D(t-\tau)}\right)e^{-\mu(t-\tau)}d\tau\\ &< 2\bar{u}_0+M.\end{aligned}$$

On the other hand, we need show that, for $h(t)\in\mathcal{S}_C$, $(\mathcal{F}h)(t)>\bar{u}_0/2$ when t is small. By Equation (2.31), we have for $0<t<t_0$

$$\begin{aligned}(\mathcal{F}h)(t) &> e^{-\mu t}\bar{I}(t)-\int_0^t\left[1-\exp\left(-\frac{r^2}{4D(t-\tau)}\right)\right]e^{-\mu(t-\tau)}k_{\text{on}}h(\tau)R_h d\tau\\ &> e^{-\mu t}3\bar{u}_0/4-k_{\text{on}}CMt.\end{aligned}$$

Hence, for $h(t)\in\mathcal{S}_C$, $(\mathcal{F}h)(t)\geq\bar{u}_0/2$ when $t<t^*$, where t^* denotes the unique root of

$$e^{-\mu t}3\bar{u}_0/4-k_{\text{on}}CMt=\bar{u}_0/2.$$

Therefore, $\mathcal{F}:\mathcal{S}_C^{t_1}\longrightarrow\mathcal{S}_C^{t_1}$ when $t_1\leq t^*$. Thus, **(A)** is verified by choosing

$$C\doteq 2\bar{u}_0+M,\ T=t_1\leq t^*. \tag{2.32}$$

□

Proof. (Proof of (B).) We will show that $\mathcal{F}$ is a contraction mapping when t is small. Choose $h_i\in\mathcal{S}_{C^*}$, $i=1,2$ and define

$$\|h_1-h_2\|_t=\max_{\tau\in[0,t]}|h_1(\tau)-h_2(\tau)|.$$

Then,

$$\begin{aligned}&|(\mathcal{F}h_1)(t)-(\mathcal{F}h_2)(t)|\\ &=\left|\int_0^t\left[1-\exp\left(-\frac{r^2}{4D(t-\tau)}\right)\right]e^{-\mu(t-\tau)}\left[K_{h_1}(\tau)-K_{h_2}(\tau)\right]d\tau\right|\\ &\leq k_{\text{on}}\int_0^t\left[1-\exp\left(-\frac{r^2}{4D(t-\tau)}\right)\right]R_{h_1}(\tau)|h_1(\tau)-h_2(\tau)|d\tau\\ &\quad+k_{\text{on}}\int_0^t\left[1-\exp\left(-\frac{r^2}{4D(t-\tau)}\right)\right]h_2(\tau)|R_{h_1}(\tau)-R_{h_2}(\tau)|d\tau\\ &\quad+k_{\text{off}}\int_0^t\left[1-\exp\left(-\frac{r^2}{4D(t-\tau)}\right)\right]|C_{h_1}(\tau)-C_{h_2}(\tau)|d\tau.\end{aligned} \tag{2.33}$$

Note that $0<R_{h_i}<M$ and $R_{h_i}+C_{h_i}=M$, $i=1,2$. Moreover, due to Equation (2.26), it is routine to derive that, for any $t>0$,

$$|R_{h_1}(t)-R_{h_2}(t)|$$

$$\leq R_0 k_{\rm on} e^{-(k_{\rm off}+k_p)t}t\|h_1-h_2\|_t+(k_{\rm off}+k_p)Mk_{\rm on}\int_0^t e^{-(k_{\rm off}+k_p)(t-\tau)}(t-\tau)d\tau\|h_1-h_2\|_t$$
$$\leq c_1\|h_1-h_2\|_t,$$

where c_1 is a constant independent of t. Because $C_{h_i}=M-R_{h_i}$, $i=1,2$, it follows immediately that for any $t>0$,

$$|C_{h_1}(t)-C_{h_2}(t)|\leq c_1\|h_1-h_2\|_t.$$

Hence, by Equation (2.33), we have

$$|(\mathcal{F}h_1)(t)-(\mathcal{F}h_2)(t)|\leq(k_{\rm on}M+k_{\rm on}Cc_1+k_{\rm off}c_1)t\|h_1-h_2\|_t.$$

Thus, $\mathcal{F}$ is a contraction mapping when

$$t<(k_{\rm on}M+k_{\rm on}Cc_1+k_{\rm off}c_1)^{-1}. \tag{2.34}$$

(B) is proved. □

In summary, by Equations (2.32) and (2.34), one easily sees that, for fixed

$$0<T<\min\left\{t_0,\ t^*,\ (k_{\rm on}M+k_{\rm on}Cc_1+k_{\rm off}c_1)^{-1}\right\},$$

$\mathcal{F}:\mathcal{S}_C^T\longrightarrow\mathcal{S}_C^T$ is a contraction mapping. According to the Banach Fixed Point Theorem, there exists a unique fixed point $h(t)\in\mathcal{S}_C^T$ of the mapping $\mathcal{F}$, namely $\mathcal{F}h=h$. In particular, due to Equation (2.30), we have the *local existence* of the positive solution to the problem (2.22). More specifically, based on previous calculations, one easily sees that the solution u can be expressed as in Equation (2.23), where $\bar{u}$ is a positive function satisfying Equation (2.24). Thus, it is standard to verify that $u(x,t)$ is locally integrable and analytic in $\mathbb{R}^2\setminus\{0\}$. The proof is complete. □

THEOREM 2.4. *Assume that the radius of the blood vessel capillary r is small, $u_0(x)\in L^\infty(\mathbb{R}^2)\bigcap C(\mathbb{R}^2)$ and $u_0(x)\geq c>0$ in $\mathbb{R}^2$.*

(i) If $k_{on}\bar{u}_0R_{3d}(0)-k_{off}C_{3d}(0)$ is positive, then, for $t>0$ small, $u(x,t)=O(\log|x|)$ for x close to 0 and $u(x,t)>0$ for $|x|>r$.

(ii) If $k_{on}\bar{u}_0R_{3d}(0)-k_{off}C_{3d}(0)$ is negative, then, for $t>0$ small, $u(x,t)=-O(\log|x|)$ for x close to 0 and $u(x,t)>ce^{-\mu t}$ in $\mathbb{R}^2$.

The proof is similar to that of [12, Theorem 2.3]. We include the details for the convenience of the reader.

Proof. According to Theorem 2.3,

$$u(x,t)=\frac{e^{-\mu t}}{4D\pi t}\int_{\mathbb{R}^2}\exp\left(-\frac{|x-y|^2}{4Dt}\right)u_0(y)dy+U(\rho,t), \tag{2.35}$$

where $\rho=|x|$ and

$$U(\rho,t)=r^2\int_0^t\frac{e^{-\mu(t-\tau)}}{4D(t-\tau)}\exp\left(-\frac{\rho^2}{4D(t-\tau)}\right)(-k_{\rm on}\bar{u}(\tau)R_{3d}(\tau)+k_{\rm off}C_{3d}(\tau))d\tau.$$

Note that for $t>0$, $u(x,t)-U(\rho,t)$ is smooth in x. Hence, it suffices to analyze the singularity of $U(\rho,t)$ for $\rho\approx0$.

From Theorem 2.3, we have

$$\begin{aligned}
U_\rho(\rho,t) &= \frac{1}{\rho}\frac{r^2}{2D}\int_0^t -\frac{\rho^2}{4D(t-\tau)^2}\exp\left(-\frac{\rho^2}{4D(t-\tau)}\right)e^{-\mu(t-\tau)} \\
&\qquad\qquad \cdot(-k_{\text{on}}\bar{u}(\tau)R_{3d}(\tau)+k_{\text{off}}C_{3d}(\tau))d\tau \\
&= \frac{1}{\rho}\frac{r^2}{2D}\int_0^t \left[\exp\left(-\frac{\rho^2}{4D(t-\tau)}\right)\right]_\tau e^{-\mu(t-\tau)}(-k_{\text{on}}\bar{u}(\tau)R_{3d}(\tau)+k_{\text{off}}C_{3d}(\tau))d\tau \\
&= \frac{1}{\rho}\frac{r^2}{2D}(-k_{\text{on}}\bar{u}(\xi)R_{3d}(\xi)+k_{\text{off}}C_{3d}(\xi))e^{-\mu(t-\xi)}\int_0^t \left[\exp\left(-\frac{\rho^2}{4D(t-\tau)}\right)\right]_\tau d\tau \\
&= \frac{1}{\rho}\frac{r^2}{2D}(k_{\text{on}}\bar{u}(\xi)R_{3d}(\xi)-k_{\text{off}}C_{3d}(\xi))e^{-\mu(t-\xi)}\exp\left(-\frac{\rho^2}{4Dt}\right),
\end{aligned}$$

where $0\le\xi\le t$. We will analyze two cases separately.

(i) Assume that $k_{\text{on}}\bar{u}_0R_{3d}(0)-k_{\text{off}}C_{3d}(0)$ is positive. Then, $k_{\text{on}}\bar{u}(t)R_{3d}(t)-k_{\text{off}}C_{3d}(t)$ remains positive for $t>0$ small due to continuity. Thus,

$$c_1(t)\frac{1}{\rho}\le U_\rho(\rho,t)\le c_2(t)\frac{1}{\rho},$$

where $c_i(t)>0$, $i=1,2$. This yields that $U_\rho(\rho,t)>0$ and

$$c_1(t)\ln\rho\le U(\rho,t)-U(1,t)\le c_2(t)\ln\rho. \tag{2.36}$$

Moreover, it is routine to verify that $U(1,t)$ is continuous in t. Therefore, by Equation (2.36), $u(x,t)=O(\log|x|)$ for x close to the origin.
Furthermore, on the one hand, $U(\rho,t)>U(r,t)$ for $\rho>r$ since $U_\rho(\rho,t)>0$. On the other hand, it is standard to verify that for t small, $|U(r,t)|<Cr^2$ with C independent of t. Hence, due to Equation (2.35) and the assumption that $u_0\ge c>0$, one easily sees that, for $|x|>r$,

$$\begin{aligned}
u(x,t) &= \frac{e^{-\mu t}}{4D\pi t}\int_{\mathbb{R}^2}\exp\left(-\frac{|x-y|^2}{4Dt}\right)u_0(y)dy+U(|x|,t) \\
&\ge ce^{-\mu t}+U(r,t)\ge ce^{-\mu t}-Cr^2>0
\end{aligned}$$

provided that r and t are small.

(ii) Assume that $k_{\text{on}}\bar{u}_0R_{3d}(0)-k_{\text{off}}C_{3d}(0)$ is negative. Similarly, $k_{\text{on}}\bar{u}(t)R_{3d}(t)-k_{\text{off}}C_{3d}(t)$ remains negative for $t>0$ small and thus

$$U(1,t)+\tilde{c}_1(t)\ln\rho\le U(\rho,t)\le U(1,t)+\tilde{c}_2(t)\ln\rho,$$

where $\tilde{c}_i(t)<0$, $i=1,2$. Hence $u(x,t)=-O(\log|x|)$ for x close to 0. At the end, due to the assumption that $k_{\text{on}}\bar{u}(0)R_{3d}(0)-k_{\text{off}}C_{3d}(0)$ is negative, by Equation (2.23), one easily sees that, for $t>0$ small, $u(x,t)>ce^{-\mu t}$ in $\mathbb{R}^2$.

The proof is complete. □

At first glance, the line-reaction model-Iseems non-physical because of the logarithmic singularity of u. However, according to Theorem 2.4, the solution $u(x,t)$ is positive in the diffusion domain (that is, when $|x|>r$). Furthermore, according to Theorem 2.3, the mean value of u in a capillary cross-section, or $\bar{u}$, is always positive. Note that it is the mean value that is used in all the reactions on the capillary, including Equations

(2.21) and (2.22) and the last term of Equation (2.19). All these facts show that the line-reaction model-Iis physical. In addition, the reaction and diffusion processes are coupled together (see Equation (2.23)), so this model satisfies criteria (C1) and (C2). Therefore, it is a valid model.

In the general case where the capillary Σ is of arbitrary shape and the tissue domain is bounded, we hypothesize that these conclusions are also true because the Dirac delta function only captures the local behavior around Σ. That is, the solution would have a logarithmic singularity on the curve Σ, and the value $\bar{u}$ would be a positive function at all time.

2.4. Two invalid models: line-reaction model-IIand -III. Sometimes, it is tempting to write the reaction-diffusion equation as (see [27])

$$\frac{\partial u}{\partial t} = D\Delta u - \mu u + \chi_\Sigma f_{3d}(u). \tag{2.37}$$

We call this line-reaction model-II. In this equation, χ_Σ is the Σ-indicator function, 1 on the one-dimensional curve Σ and 0 otherwise. This equation models the reaction only on the capillary centerline Σ. Because u is used in the reaction, it should be finite on Σ according to the criterion (C1) in Section 2. Thus, if Equation (2.37) is integrated over the whole domain Ω, the last term will disappear because Σ is of zero measure in Ω. This suggests that the reaction term has no contribution to the ligand rate of change in Ω at all. Therefore, this equation is invalid according to the criterion (C2).

Compared with Equation (2.19) and Equation (2.37), it is more tempting to write an equation (e.g., [33])

$$\frac{\partial u}{\partial t} = D\Delta u - \mu u + \delta_\Sigma f_{3d}(u) \quad \text{for } x \in \mathbb{R}^3, t > 0. \tag{2.38}$$

We call this line-reaction model-III. In this equation, the reaction also occurs on the capillary centerline only. This model seems better than Equation (2.37) because the integration over the whole domain does not seem to eliminate the reaction term. According to the criterion (C1), it is expected that u is finite on Σ. Furthermore, we expect u to be continuous in space and time because it is awkward to see a finite but discontinuous growth factor concentration. However, this could not be achieved by model (2.38), which can be seen from the following analysis.

For simplicity, we assume that the capillary radius is a constant, say r, then the definition of the line delta function (2.20) becomes, $\forall \phi(x) \in \mathcal{S}(\mathbb{R}^3)$,

$$\int_{\mathbb{R}^3} \delta_\Sigma(x)\phi(x)dx = \pi r^2 \int_0^1 |\gamma'(s)|\phi(\gamma(s))ds,$$

where $\Sigma = \gamma([0,1])$.

THEOREM 2.5. *Given a continuous function f in $\mathbb{R}$ and a bounded and continuous function $u_0(x) \geq 0$ in $\mathbb{R}^3$, assume that $u_0 \in L^1(\mathbb{R}^3)$ and $f(u_0(x))$ is not identically zero on Σ. Then the model (2.38) does not admit a solution $u(x,t) \in C(\mathbb{R}^3 \times [0,T])$, $T > 0$ with $u(x,0) = u_0(x)$ in $\mathbb{R}^3$.*

Proof. Suppose the conclusion is not true, i.e., that Equation (2.38) admits a solution $u(x,t) \in C(\mathbb{R}^3 \times [0,T])$ for some $T > 0$ with $u(x,0) = u_0(x)$ in $\mathbb{R}^3$ and that f and u_0 satisfy the conditions in Theorem 2.5. Similar to the computation in [12], by the Fourier transform, the solution of the model (2.38) can be expressed as follows:

$$u(x,t) = e^{-\mu t} \int_{\mathbb{R}^3} \frac{1}{(4\pi D t)^{3/2}} \exp\left(-\frac{|x-y|^2}{4Dt}\right) u_0(y)dy$$

$$
\begin{aligned}
&+\int_0^t\int_{\mathbb{R}^3}\frac{e^{-\mu(t-\tau)}}{(4\pi D(t-\tau))^{3/2}}\exp\left(-\frac{|x-y|^2}{4D(t-\tau)}\right)\delta_\Sigma(y)f_{3d}(u(y,\tau))dyd\tau\\
&=e^{-\mu t}\int_{\mathbb{R}^3}\frac{1}{(4\pi Dt)^{3/2}}\exp\left(-\frac{|x-y|^2}{4Dt}\right)u_0(y)dy\\
&\quad+\int_0^t\int_0^1\frac{\pi r^2e^{-\mu(t-\tau)}}{(4\pi D(t-\tau))^{3/2}}\exp\left(-\frac{|x-\gamma(s)|^2}{4D(t-\tau)}\right)|\gamma'(s)|f_{3d}(u(\gamma(s),\tau))dsd\tau,
\end{aligned}
$$

for $0<t<T$.

According to the conditions in Theorem 2.5, without loss of generality assume that there exist $\ell\in(0,1)$, $\epsilon>0$, and $\delta>0$ such that $[\ell-\epsilon,\ell+\epsilon]\subset[0,1]$ and $|\gamma(\ell)-\gamma(s)|\geq\delta$ for $|\ell-s|>\epsilon$ and

$$
f_{3d}(u(\gamma(s),t))>c_0\quad\text{for } s\in[\ell-\epsilon,\ell+\epsilon],\ 0\leq t\leq t_0,
$$

where $0<t_0<T$ and $c_0>0$. Denote

$$
c_1=\min_{0\leq s\leq 1}|\gamma'(s)|,\quad c_2=\max_{0\leq s\leq 1}|\gamma'(s)|.
$$

It is clear that $0<c_1<c_2<\infty$ since $\Sigma=\gamma([0,1])$ is a smooth curve. Then, we have for $0\leq t\leq t_0$

$$
\begin{aligned}
&u(\gamma(\ell),t)\\
&\geq e^{-\mu t}\int_{\mathbb{R}^3}\frac{1}{(4\pi Dt)^{3/2}}\exp\left(-\frac{|\gamma(\ell)-y|^2}{4Dt}\right)u_0(y)dy\\
&+c_0c_1\int_0^t\int_{\ell-\epsilon}^{\ell+\epsilon}\frac{\pi r^2e^{-\mu(t-\tau)}}{(4\pi D(t-\tau))^{3/2}}\exp\left(-\frac{|\gamma(\ell)-\gamma(s)|^2}{4D(t-\tau)}\right)dsd\tau\\
&-c_2\int_0^t\left(\int_0^{\ell-\epsilon}+\int_{\ell+\epsilon}^1\right)\frac{\pi r^2e^{-\mu(t-\tau)}}{(4\pi D(t-\tau))^{3/2}}\exp\left(-\frac{\delta^2}{4D(t-\tau)}\right)|f_{3d}(u(\gamma(s),\tau))|dsd\tau. \quad (2.39)
\end{aligned}
$$

Now, by Equation (2.39), one sees that, to derive a contradiction, it suffices to show that

$$
\int_0^t\int_{\ell-\epsilon}^{\ell+\epsilon}\frac{1}{(4\pi D(t-\tau))^{3/2}}\exp\left(-\frac{|\gamma(\ell)-\gamma(s)|^2}{4D(t-\tau)}\right)dsd\tau=+\infty. \quad (2.40)
$$

Direct computation yields that

$$
\begin{aligned}
&\int_0^t\int_{\ell-\epsilon}^{\ell+\epsilon}\frac{1}{(4\pi D(t-\tau))^{3/2}}\exp\left(-\frac{|\gamma(\ell)-\gamma(s)|^2}{4D(t-\tau)}\right)dsd\tau\\
&=\int_0^t\int_{-\epsilon}^{\epsilon}\frac{1}{(4\pi D\tau)^{3/2}}\exp\left(-\frac{|\gamma'(\xi)|^2s^2}{4D\tau}\right)dsd\tau\\
&=\int_0^t\int_{-\frac{|\gamma'(\xi)|}{\sqrt{4D\tau}}\epsilon}^{\frac{|\gamma'(\xi)|}{\sqrt{4D\tau}}\epsilon}\frac{1}{|\gamma'(\xi)|\sqrt{\pi}}\frac{1}{4\pi D\tau}\exp\left(-\eta^2\right)d\eta d\tau\\
&\geq\int_0^t\frac{1}{|\gamma'(\xi)|}\frac{1}{4\pi D\tau}\sqrt{1-\exp\left(-\frac{|\gamma'(\xi)|^2}{4D\tau}\epsilon^2\right)}d\tau=+\infty
\end{aligned}
$$

where $\xi\in[\ell-\epsilon,\ell+\epsilon]$. Therefore, Equation (2.40) is verified and the proof is complete.□

This proof shows that, if the reaction rate $f_{3d}(u)$ becomes nonzero on some point of Σ at one moment, then the local value u there will blow up immediately. In general, the reaction rate is nonzero in the biological process. Therefore, this model creates singularity on the capillary centerline. Because the local value of u on the centerline is used in the reactions, this model is invalid according to the criterion (C1). On the other hand, if $f_{3d}(u)$ is identically zero on Σ for all time, then this singularity will disappear. However, this is equivalent to removing the reaction term $\delta_\Sigma f_{3d}(u)$ from the modeling Equation (2.38). In this case, the function $f_{3d}(u)=0$ itself indicates the value u on Σ and the diffusion has no effects on it at all. According to the criterion (C2), the model is also invalid. Therefore, no matter what the $f_{3d}(u)$ value is (either identically zero or not) this model is invalid.

In contrast, although the local value u is also singular in the line-reaction model-I, the mean value on the capillary cross-section is finite and positive, and it is the mean value that is utilized in the reactions. Consequently, the line-reaction model-Iis valid.

3. Comparison in numerical implementation

In numerical implementations, the volume-reaction and line-reaction models are superior to the surface-reaction models in programming complexity and computational cost when handling large domains and a large number of blood capillaries of complex shapes. This is mainly because the surface-reaction models require us to explicitly construct the capillary surface but the volume-reaction and line-reaction models do not.

Among surface-reaction models, there exist two numerical approaches to construct the blood capillary surface. The first approach directly generates a mesh on the capillary surface, as in [5, 15, 17]. These models just study one single cell and its nearby region whose domain size is a few dozen microns. Another approach uses intersections of the diffusion mesh lines and capillary surface whose analytic form is given, as in [13, 14]. In these two works, the domain is $200\times200\times800\,\mu m^3$, the capillary diameter is $6\,\mu m$ and the mesh size is $1\,\mu m$ in each spatial coordinate, which lead to roughly 3×10^7 mesh points. When the domain size is increased to millimeters, capturing the surface of very thin capillaries and implementing surface boundary conditions become very challenging. Comparing with the work of [13, 14], if the the domain is enlarged to $2000\times2000\times800\,\mu m^3$ with the same mesh size, then it requires 3×10^9 mesh points, which would be too expensive to implement. Furthermore, the surface-reaction models have to identify the tissue domain outside the capillaries to discretize the diffusion term. The flux boundary condition has to be applied on the capillary surface mesh points. If the surface mesh points do not coincide with the diffusion mesh points, then a special treatment of the finite differencing of the diffusion term around the capillary has to be designed (for example see [4,13]). All these increase the difficulty in computer programming of the surface-reaction models.

In contrast, the volume-reaction and line-reaction models do not need to track the capillary surface. In all these models, a sequence of discrete points is used to denote the capillary centerline and a radius is assigned to the capillaries, as in [3, 6, 10, 16, 19, 28, 29, 31, 33]. The (mollified) Heaviside function or (mollified) Dirac delta function is spread over diffusion mesh points according to the capillary centerline location and radius. In this manner, these models not only save the construction of capillary surface or volume but allow rather coarse meshes of the tissue domain, which could significantly reduce the computational cost. For instance, comparing with the work of [13,14], if the the domain is enlarged to $2000\times2000\times800\,\mu m^3$ with the mesh size $10\,\mu m$, then the volume-reaction and line-reaction models can still capture the contribution from the

capillaries through the use of the mollified Heaviside or delta function, but they keep the mesh points down to 3×10^7. The surface-reaction models would have trouble with this mesh resolution because a capillary of diameter $6\mu m$ might not be intersected by mesh lines $10\mu m$ apart. Therefore, the volume-reaction and line-reaction models can handle domains as large as a few millimeters or larger in diameter where hundreds to thousands of tortuous capillaries form a dense network. Furthermore, there is no boundary condition or special finite differencing required around the capillary, and the diffusion term is discretized everywhere the same. Thus, the computer programming of the volume-reaction and line-reaction models is far easier.

4. Comparison in prediction of growth factor dynamics

To study the quantitative differences between the surface-reaction models and the volume/line-reaction models, we construct a simple radially symmetric two-dimensional problem. We take a cross-section of a capillary of radius r and the surrounding tissue of radius R, where $r \ll R$. We impose the no-flux boundary condition on the outer circle. The solution is denoted as $u(\rho,t)=u(x,t)$, where $x=(x_1,x_2)$ and the radius coordinate $\rho=\sqrt{x_1^2+x_2^2}$. The surface-reaction model for this problem is written as

$$\textbf{Problem 1:}\quad \left\{\begin{array}{rl} \frac{\partial u}{\partial t} &= D\frac{1}{\rho}\frac{\partial}{\partial\rho}\left(\rho\frac{\partial u}{\partial\rho}\right)-\mu u, \quad r<\rho<R,\\ D\frac{\partial u}{\partial\rho}|_{\rho=r} &= -f_{2d}(u,R_{2d},C_{2d})=k_{\rm on}uR_{2d}-k_{\rm off}C_{2d},\\ D\frac{\partial u}{\partial\rho}|_{\rho=R} &= 0,\\ \frac{dR_{2d}}{dt} &= -k_{\rm on}uR_{2d}+k_{\rm off}C_{2d}+k_pC_{2d},\\ \frac{dC_{2d}}{dt} &= k_{\rm on}uR_{2d}-k_{\rm off}C_{2d}-k_pC_{2d},\\ u(\rho,t=0) &= U, \quad 0\le\rho\le R,\\ R_{2d}(t=0) &= \frac{r}{2}R_T, \quad C_{2d}(t=0)=0. \end{array}\right\} \tag{4.1}$$

Note that in Problem 1, the quantities R_{2d} and C_{2d} are only defined on $\rho=r$. Since the volume-reaction model and line-reaction model-Iare equivalent under the numerical method used in this study (see Appendix B), we only list the volume-reaction model below.

$$\textbf{Problem 2:}\left\{\begin{array}{rl} \frac{\partial u}{\partial t} &= D\frac{1}{\rho}\frac{\partial}{\partial\rho}\left(\rho\frac{\partial u}{\partial\rho}\right)-\mu u+\chi_{\Omega_C}f_{3d}(u,R_{3d},C_{3d}), 0<\rho<R,\\ f_{3d}(u,R_{3d},C_{3d}) &= -k_{\rm on}uR_{3d}+k_{\rm off}C_{3d},\\ D\frac{\partial u}{\partial\rho}|_{\rho=0} &= D\frac{\partial u}{\partial\rho}|_{\rho=R}=0,\\ \frac{\partial R_{3d}}{\partial t} &= -k_{\rm on}\bar{u}R_{3d}+k_{\rm off}C_{3d}+k_pC_{3d}, \quad 0\le\rho\le r,\\ \frac{\partial C_{3d}}{\partial t} &= k_{\rm on}\bar{u}R_{3d}-k_{\rm off}C_{3d}-k_pC_{3d}, \quad 0\le\rho\le r,\\ u(\rho,t=0) &= U, \quad 0\le\rho\le R,\\ R_{3d}(\rho,t=0) &= R_T, \quad C_{3d}(\rho,t=0)=0, \quad 0\le\rho\le r. \end{array}\right\} \tag{4.2}$$

We denote the solution of Problem 1 as $(u_1,R_{1,2d},C_{1,2d})$ and that of Problem 2 as (u_2,R_2,C_2) and then define $R_1=\frac{2}{r}R_{1,2d}$ and $C_1=\frac{2}{r}C_{1,2d}$. To estimate the difference between Problem 1 and Problem 2, we introduce the following errors:

$$||E_u||_{\max,T}=\max_{\rho\in[r,R]}\frac{|u_1(\rho,T)-u_2(\rho,T)|}{|u_1(\rho,T)|}, ||E_u||_{\max,r}=\max_{t\in[0,T]}\frac{|u_1(r,t)-u_2(r,t)|}{|u_1(r,t)|}, \tag{4.3}$$

$$||E_R||_{\max,r}=\max_{t\in[0,T]}\frac{|R_1(t)-R_2(t)|}{|R_1(t)|}, ||E_C||_{\max,r}=\max_{t\in[0,T]}\frac{|C_1(t)-C_2(t)|}{|C_1(t)|}. \tag{4.4}$$

The numerical methods of Problem 1 and Problem 2 are shown in Appendix B. In our test, we set $T = 4.8$ hours. All the parameter values are given in Table 4.1. Note the control values and the ranges of parameters are not only valid for VEGF, but also used for epidermal growth factor (EGF) (see [17]).

Parameter	Variable	Control Value	Range	Source
Capillary radius	r	$10\mu m$	$2 \sim 20\mu m$	[26]
Tissue radius	R	$2mm$	fixed	[7, 26]
Diffusion constant	D	$10^{-6} cm^2 s^{-1}$	$10^{-10} \sim 10^{-3} cm^2 s^{-1}$	[15, 17]
Decay rate	μ	$1.8 \times 10^{-4} s^{-1}$	$1.8 \times 10^{-7} \sim 3.6 \times 10^{-4} s^{-1}$	[25]
Association rate	k_{on}	$1.2 \times 10^6 M^{-1} s^{-1}$	$1.2 \times 10^5 \sim 1.2 \times 10^8 M^{-1} s^{-1}$	[15, 17]
Dissociation rate	k_{off}	$4.1 \times 10^{-4} s^{-1}$	$4.1 \times 10^{-6} \sim 4.1 \times 10^{-2} s^{-1}$	[15, 17]
Internalization rate	k_p	$2.8 \times 10^{-4} s^{-1}$	$10^{-6} \sim 10^{-2} s^{-1}$.	[15]
VEGF reference value	U	$2.22 \times 10^{-3} \mu M$	$10^{-6} \sim 10^{-1} \mu M$	[15]
VEGFR2 concentration	R_T	$1.3 \times 10^{-3} \mu M$	$4 \times 10^{-4} \sim 4 \times 10^{-3} \mu M$	[5, 9, 15]

TABLE 4.1. *Parameters*

First, we pick up eight parameters to study their effects on the difference between Problem 1 and Problem 2: diffusion constant D, decay rate μ, association rate k_{on}, disassociation rate k_{off}, internalization rate k_p, capillary radius r, VEGF reference value U (used as the initial value), and VEGFR2 total concentration R_T. When testing each of these parameters, we fix all other parameters as the control values in Table 4.1 and choose some values of the tested parameter well spread in its range. The results are shown in Figure 4.1. Among all these eight parameters, the diffusion constant has the most remarkable impact on the difference between these two models. When D is reduced to $10^{-10} cm^2 s^{-1}$, the smallest value in its range, the solution of Problem 2 differs significantly from that of Problem 1 near the capillary (Figure 4.1[a]): the maximum relative errors reach about 37%. Among three kinetics parameters, the association rate k_{on} is most significant: the difference is larger when k_{on} is increased, but it is still less than 1% (Figure 4.1[c]). Although the differences are larger when the capillary radius r and the total VEGFR2 concentration R_T are enlarged, the magnitude of the differences is less than 0.1% (Figure 4.1[f][h]). The decay rate μ and VEGF reference value U have negligible effects on the difference between the two models (Figure 4.1[b][g]).

Next, we focus on the diffusion constant and show the details of results when $D = 10^{-6} cm^2 s^{-1}$ and $10^{-10} cm^2 s^{-1}$ in Figure 4.2 and Figure 4.3, respectively. All other parameters are of the control values in Table 4.1. When $D = 10^{-6} cm^2 s^{-1}$, the solutions of Problem 1 and Problem 2 almost coincide (Figure 4.2), but, when $D = 10^{-10} cm^2 s^{-1}$, the solutions differ significantly (Figure 4.3). One may notice the decrease of u when D is reduced (comparing Figure 4.2[a] and Figure 4.3[a]). This is because the compensation of the loss of growth factor due to reaction is less when the diffusion constant is smaller.

Although the parameters are chosen for VEGF, the comparison results are similar for many other growth factors in angiogenesis, such as Platelet-derived growth factor (PDGF) and angiopoietins, (see models in [32]) and growth factors in general cell biology, such as epidermal growth factor (EGF) ([17]).

5. Conclusions

This work is the first time when a comprehensive comparison of existing reaction and diffusion models of growth factors in angiogenesis has been presented. These models include one surface-reaction model, one volume-reaction model, and three line-reaction models, which have represented all current mathematical models using partial differential equations in this research field. The reactions in these models are the binding

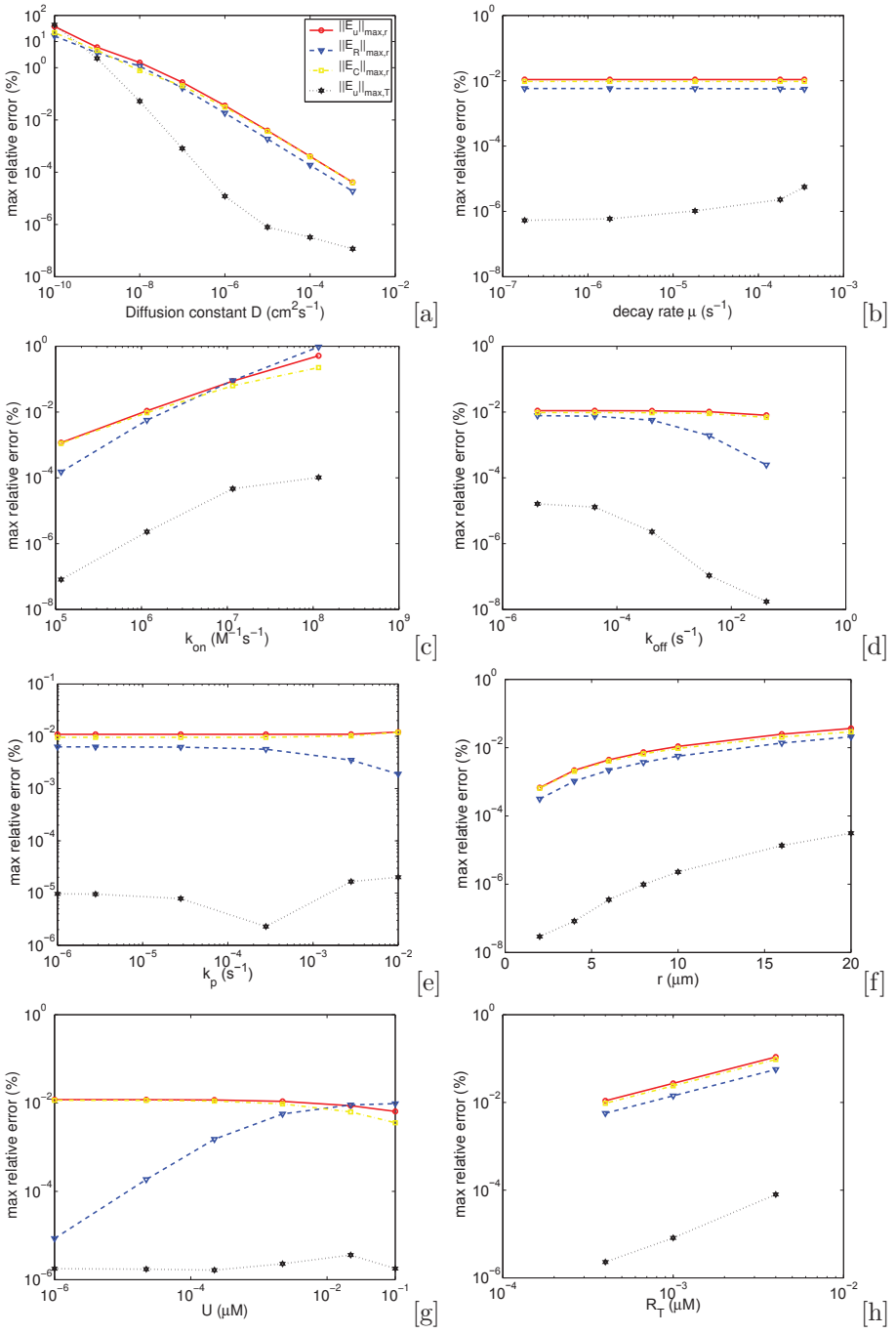

FIG. 4.1. *Errors for various values of D, μ, k_{on}, k_{off}, k_p, r, U, and R_T. The legends are the same for all these figures.*

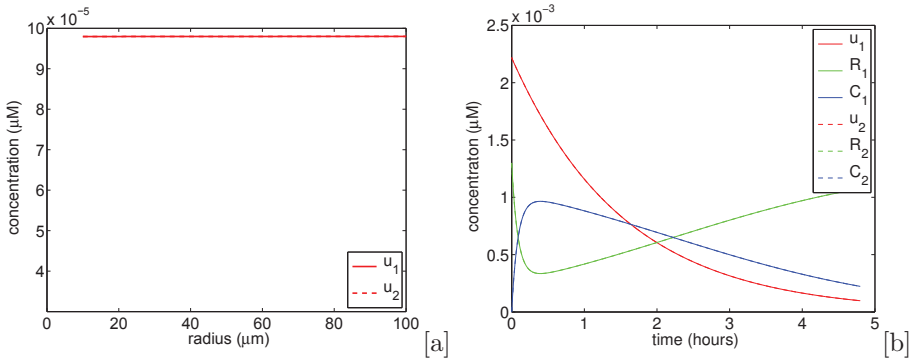

FIG. 4.2. *[a]&[b]: $D=10^{-6}cm^2s^{-1}$. [a]: u at $t=4.8$ hours. [b]: Solutions at $\rho=r$. Note the solution curves of the same variables in different problems are indistinguishable in these figures.*

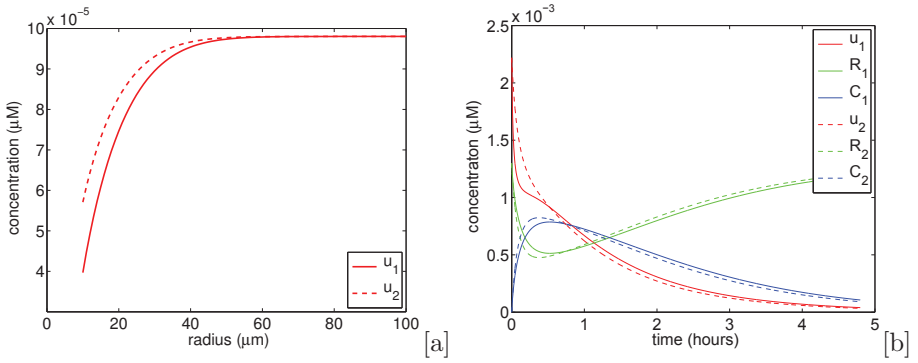

FIG. 4.3. *[a]&[b]: $D=10^{-10}cm^2s^{-1}$. [a]: u at $t=4.8$ hours. [b]: Solutions at $\rho=r$.*

kinetics between growth factors and receptors on the capillary surface. Therefore, the precise location of reactions is the capillary surface. In this sense, the surface-reaction model is the most realistic and accurate one, while the volume-reaction and line-reaction models lump the reactions to the capillary volume or centerline, which can be regarded as approximations or simplified models of the surface-reaction model. The complexity of the surface-reaction model in computation justifies the development of these simplified models. An important contribution of this paper is to point out that some of the simplified models in the literature may be problematic mathematically. We compared these models in the following three aspects.

First, we mainly studied the qualitative features of these models, including solution existence, regularity and positivity. The qualitative features of these models are briefly summarized in Table 2.1. The solution of the surface-reaction model is smooth and positive and has higher regularity than any other valid models studied in this work. In the volume-reaction model, a Heaviside (characteristic) function is used to represent the capillary volume, and the solution is positive and has second order spatial derivatives in the weak sense.

In terms of modeling simplicity, the line-reaction models are most attractive because the reactions are only occurring on a one-dimensional curve (capillary centerline). It is especially interesting to study the qualitative features of the line-reaction model-Iand -IIIbecause they use the unknown solution with the Dirac delta function as the line source, which is new in the literature. The model-IIIuses the local value of the

unknown solution, which either blows up or annihilates the line source. Thus, the model-IIIis invalid. In contrast, the model-Iuses the mean value of the unknown solution in a region around the capillary centerline. We prove that this mean value is finite and positive and the reaction and diffusion processes are coupled together. Thus, the model-Iis valid. This comparison implies that using the local value of the unknown solution is too demanding for the Dirac delta line source, while the mean value relaxes this stringency.

Second, we briefly compared the computer implementations of these models. In the current literature, the surface-reaction model has only been applied to domains from a few dozen microns to a few hundred microns in size. When the domain size is increased to a few millimeters or above, the volume-reaction models or line-reaction models take over. This is mainly because the surface-reaction models require us to identify and resolve the capillary surface, which increases the programming complexity and computational cost.

Third, we quantitatively compared the prediction in growth factor dynamics of these models using one typical reaction diffusion problem. It turns out that the volume-reaction model and the line-reaction model-Iare satisfactory approximations of the surface-reaction model in most parameter value ranges. However, when the diffusion constant is very small, these two models present significant deviation from the surface-reaction model.

As theoretical models, the surface-reaction model is the most accurate and delicate, the line-reaction model-Iis the simplest, and the volume-reaction model lies in between. As numerical models, the surface-reaction model is the most complicated and suitable for small domains, while the volume-reaction model and line-reaction model-Iare simpler and recommended for large domains with a large number of capillaries.

Appendix A. Proof of boundary condition $\mathbf{J}_F(u)\cdot\mathbf{n}=-f_{2d}(u)$.

THEOREM A.1. *If u is smooth and $|\frac{du}{dt}|$ and $|\nabla u|$ are bounded, then $\mathbf{J}_F\cdot\mathbf{n}=-f_{2d}(u)$ on $\partial\Omega_C$ where $\mathbf{n}$ is the unit normal vector on $\partial\Omega_C$ pointing to the interior of Ω_C.*

Proof. At any point $x\in\partial\Omega_C$, select a control volume $V\subset\Omega_T$ whose lower surface S_l belongs to $\partial\Omega_C$ and centers around x, and the upper surface S_u is obtained by shifting the lower surface outward by a distance ϵ (see Figure A.1). Denote the side surface of V as S_s. Suppose the area of S_l is equal to A and the perimeter of S_l is less than $10\sqrt{A}$. Then, the volume of V is $\leq 2\epsilon A$ and the area of S_s is $\leq 10\epsilon\sqrt{A}$. Let the outward unit normal vector on ∂V be $\mathbf{n}$, which is the same as that of $\partial\Omega_c$ when restricted on S_l.

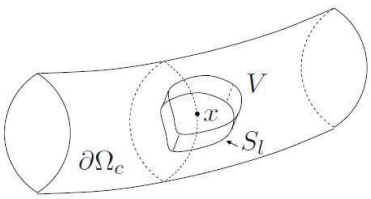

FIG. A.1. *Control volume V intersects with $\partial\Omega_c$ at the surface S_l.*

The mass conservation equation of u in V is

$$\frac{d}{dt}\int_V u dV=-\int_{S_u\cup S_s}\mathbf{J}_F\cdot\mathbf{n}dS+\int_{S_l}f_{2d}dS.$$

Suppose $|\frac{du}{dt}|$ and $|\nabla u|$ are bounded by a constant $M>0$. Then the mean value theorem suggests that $|\frac{d}{dt}\int_V u dV| \le \epsilon ADM$, $\int_{S_u} \mathbf{J}_F \cdot \mathbf{n} dS = A(\mathbf{J}_F \cdot \mathbf{n})(\xi_1)$, $\int_{S_l} f_{2d}(u) dS = A f_{2d}(u(\xi_2))$, $|\int_{S_s} \mathbf{J}_F \cdot \mathbf{n} dS| \le 10\epsilon M\sqrt{A}$, where $\xi_1 \in S_u$ and $\xi_2 \in S_l$. Let $\epsilon \to 0$. Then, we obtain

$$\mathbf{J}_F \cdot \mathbf{n}(\xi_1) = -f_{2d}(u(\xi_2)).$$

Note the limit of ξ_1 lies on S_l and therefore the normal vector at ξ_1 switches direction when going from S_u to S_l. Let $A \to 0$, then $\xi_1 \to x$, and $\xi_2 \to x$, so $\mathbf{J}_F \cdot \mathbf{n} = -f_{2d}(u)$ at x. ∎

Appendix B. Finite volume method for Problem 1 and Problem 2. The only difference between the volume-reaction model and the line-reaction model-Ilies in the equation of the growth factor, namely Equation (2.14) and Equation (2.19). Although these two equations are distinct in their differential forms and positivity of u, there is not much difference in numerical implementations. Indeed, it can be proven that they are identical in the following finite volume method. Let $\mathcal{M}$ be a finite family of non-empty connected open disjoint subsets of Ω (the finite volumes) such that $\overline{\Omega} = \cup_{V \in \mathcal{M}} \overline{V}$. On each $V \in \mathcal{M}$, a general reaction diffusion equation

$$\frac{\partial u}{\partial t} = D\Delta u - \mu u + F(u)$$

is integrated over V to obtain

$$\int_V \frac{\partial u}{\partial t} dx = \int_{\partial V} \hat{\mathbf{J}}_F \cdot \mathbf{n} dS - \mu \int_V u dx + \int_V F(u) dx$$

where $\hat{\mathbf{J}}_F$ is the numerical Fickian flux on ∂V. Denote the mean value on each finite volume V as $\bar{u}_V$, namely $\bar{u}_V \triangleq \frac{1}{|V|}\int_V u dx$. If we approximate $\int_V F(u) dx$ by $\int_V F(\bar{u}_V) dx$, then the finite volume method is

$$\frac{d\bar{u}_V}{dt} = \frac{1}{|V|}\int_{\partial V} \hat{\mathbf{J}}_F \cdot \mathbf{n} dS - \mu \bar{u}_V + \frac{1}{|V|}\int_V F(\bar{u}_V) dx.$$

We choose one special type of finite volumes which satisfies the following condition.

Definition B.1. *A finite volume discretization* $\{\mathcal{M}\}$ *satisfies the* **capillary segmentation condition** *if any finite volume* $V \in \mathcal{M}$ *intersecting with the capillary is a segment of the capillary, that is, its two ends are two cross-sections of the capillary and the side boundary belongs to the capillary surface* $\partial\Omega_C$.

In Equation (2.14), $F(u) = \chi_{\Omega_C} f_{3d}(u)$, so $\frac{1}{|V|}\int_V \chi_{\Omega_C} f_{3d}(\bar{u}_V) dx = f_{3d}(\bar{u}_V)$ if V is a capillary segment and 0 otherwise. In Equation (2.19), $f(u) = \delta_\Sigma f_{3d}(\bar{u})$, so $\frac{1}{|V|}\int_V \delta_\Sigma f_{3d}(\bar{u}_V) dx = f_{3d}(\bar{u}_V)$ if V is a capillary segment and 0 otherwise. Therefore, the finite volume discretizations are identical for these two models. This result can be summarized below.

Proposition B.1. *In the finite volume method satisfying the capillary segmentation condition, the modeling equations (2.14) and (2.19) have the same form:*

$$\frac{d\bar{u}_V}{dt} = \frac{1}{|V|}\int_{\partial V} \hat{\mathbf{J}}_F \cdot \mathbf{n} dS - \mu \bar{u}_V + \begin{cases} f_{3d}(\bar{u}_V), & \text{if } V \text{ is a capillary segment;} \\ 0, & \text{otherwise.} \end{cases}$$

Note that this finite volume method only computes the mean value in an entire capillary segment or cross-section. According to Theorem 2.3, this mean value is always positive. Therefore, this numerical method will not capture the negative value or the singularity near the capillary centerline in the line-reaction model-I. However, if a sufficient numerical discretization is utilized inside the capillary segment or cross-section, then the negative value of the line-reaction model-Ican be captured, as in [12]. The reason why we only compute the mean value in this work is that only the mean value is required in the reactions on the capillary in the line-reaction model-I(see equations in (2.19)).

The details of numerical implementation of Problem 1 and Problem 2 are as follows. The forward Euler scheme with time step size Δt is applied for the temporal discretization. Along the radial direction, an n-subdivision with $n+1$ mesh points $\rho_1 < \cdots < \rho_{n+1}$ is assigned. For Problem 1, $\rho_1 = r$, $\rho_{n+1} = R$, and the mesh size $\rho_{i+1} - \rho_i = \frac{R-r}{n}, i = 1,\ldots,n$. For Problem 2, $\rho_1 = 0$, $\rho_2 = r$, $\rho_{n+1} = R$, $\rho_{i+1} - \rho_i = \frac{R-r}{n-1}, i = 2,\ldots,n$.

For a finite volume $V_i = (\rho_i, \rho_{i+1}) \times (0, 2\pi)$, we define the mean value of u as

$$\bar{u}_i = \frac{1}{\pi(\rho_{i+1}^2 - \rho_i^2)} \int_{\rho_i}^{\rho_{i+1}} \int_0^{2\pi} \rho u(\rho,\theta,t) d\rho d\theta = \frac{2}{(\rho_{i+1}^2 - \rho_i^2)} \int_{\rho_i}^{\rho_{i+1}} \rho u(\rho,t) dr.$$

Denote the solution at t^k as $\bar{u}_i^k$, and we are going to solve $\bar{u}_i^{k+1}, i = 1, \cdots, n$. The numerical scheme is the same for Problem 1 and Problem 2 when $i = 2,\ldots,n$. In $V_i, i = 2,\ldots,n$, for both Problem 1 and Problem 2, we have $\frac{\partial u}{\partial t} = D\frac{1}{\rho}\frac{\partial}{\partial \rho}\left(\rho \frac{\partial u}{\partial \rho}\right) - \mu u$. Thus,

$$\frac{d\bar{u}_i}{dt} = \frac{2}{(\rho_{i+1}^2 - \rho_i^2)} \left(D\left(\rho_{i+1} \frac{\partial u}{\partial \rho}|_{\rho_{i+1}} - \rho_i \frac{\partial u}{\partial \rho}|_{\rho_i} \right) - \mu \int_{\rho_i}^{\rho_{i+1}} \rho u d\rho \right).$$

We approximate $\frac{d\bar{u}_i}{dt}$ by $\frac{\bar{u}_i^{k+1} - \bar{u}_i^k}{\Delta t}$, $\frac{\partial u}{\partial \rho}|_{\rho_i}$ by $\frac{\bar{u}_i^{k+1} - \bar{u}_{i-1}^{k+1}}{(\rho_{i+1} - \rho_{i-1})/2}$ and $\int_{\rho_i}^{\rho_{i+1}} \rho u d\rho$ by $\frac{\rho_{i+1}^2 - \rho_i^2}{2} \bar{u}_i^{k+1}$. The numerical scheme for $i = 2,\ldots,n-1$ is

$$\begin{aligned}
&\frac{-4D\rho_i \Delta t}{(\rho_{i+1}^2 - \rho_i^2)(\rho_{i+1} - \rho_{i-1})} \bar{u}_{i-1}^{k+1} \\
&+ \left(1 + \frac{4D\rho_i \Delta t}{(\rho_{i+1}^2 - \rho_i^2)(\rho_{i+1} - \rho_{i-1})} + \frac{4D\rho_{i+1} \Delta t}{(\rho_{i+1}^2 - \rho_i^2)(\rho_{i+2} - \rho_i)} + \mu \Delta t \right) \bar{u}_i^{k+1} \\
&+ \frac{-4D\rho_{i+1} \Delta t}{(\rho_{i+1}^2 - \rho_i^2)(\rho_{i+2} - \rho_i)} \bar{u}_{i+1}^{k+1} = \bar{u}_i^k.
\end{aligned}$$

When $i = n$, using the boundary condition $\frac{\partial u}{\partial r}|_{\rho_{n+1}} = 0$, we get

$$\frac{-4D\rho_n \Delta t}{(\rho_{n+1}^2 - \rho_n^2)(\rho_{n+1} - \rho_{n-1})} \bar{u}_{n-1}^{k+1} + \left(1 + \frac{4D\rho_n \Delta t}{(\rho_{n+1}^2 - \rho_n^2)(\rho_{n+1} - \rho_{n-1})} + \mu \Delta t \right) \bar{u}_n^{k+1} = \bar{u}_i^k.$$

For Problem 1, when $i = 1$, using the boundary condition $D\frac{\partial u}{\partial r}|_r = -f_{2d}$, we achieve

$$\begin{aligned}
&\left(1 + \frac{4D\rho_2 \Delta t}{(\rho_2^2 - \rho_1^2)(\rho_3 - \rho_1)} + \mu \Delta t \right) \bar{u}_1^{k+1} + \frac{-4D\rho_2 \Delta t}{(\rho_2^2 - \rho_1^2)(\rho_3 - \rho_1)} \bar{u}_2^{k+1} \\
&= \bar{u}_1^k + \frac{2\rho_1 \Delta t}{\rho_2^2 - \rho_1^2} f_{2d}(\bar{u}_1^k, R_{2d}^k, C_{2d}^k).
\end{aligned}$$

For Problem 2, when $i=1$, the integration of $\chi_{\Omega_C} f_{3d}$ over V_1 is $\pi(\rho_2^2-\rho_1^2)f_{3d}$. Therefore,

$$\left(1+\frac{4D\rho_2\Delta t}{(\rho_2^2-\rho_1^2)(\rho_3-\rho_1)}+\mu\Delta t\right)\bar{u}_1^{k+1}+\frac{-4D\rho_2\Delta t}{(\rho_2^2-\rho_1^2)(\rho_3-\rho_1)}\bar{u}_2^{k+1}=\bar{u}_1^k+\Delta t f_{3d}(\bar{u}_1^k,R_{3d}^k,C_{3d}^k).$$

The free and bound receptors are solved using the same scheme in these two problems:

$$\begin{aligned}
R_{2d}^{k+1}&=R_{2d}^k+\Delta t\left(-k_{\text{on}}\bar{u}_1^k R_{2d}^k+(k_{\text{off}}+k_p)C_{2d}^k\right),\\
C_{2d}^{k+1}&=C_{2d}^k-\Delta t\left(-k_{\text{on}}\bar{u}_1^k R_{2d}^k+(k_{\text{off}}+k_p)C_{2d}^k\right),\\
R_{3d}^{k+1}&=R_{3d}^k+\Delta t\left(-k_{\text{on}}\bar{u}_1^k R_{3d}^k+(k_{\text{off}}+k_p)C_{3d}^k\right),\\
C_{3d}^{k+1}&=C_{3d}^k-\Delta t\left(-k_{\text{on}}\bar{u}_1^k R_{3d}^k+(k_{\text{off}}+k_p)C_{3d}^k\right).
\end{aligned}$$

In the examples of Section 4, $r=0.01mm$, $R=2mm$, $n=2000$ for Problem 1 and $n=2001$ for Problem 2, and $\Delta t=10^{-6}days$.

REFERENCES

[1] A.R.A. Anderson and M.A.J. Chaplain, *Continuous and discrete mathematical models of tumor-induced angiogenesis*, Bull. Math. Biol., 60, 857–900, 1998.

[2] F. Billy, B. Ribba, O. Saut, H. Morre-Trouilhet, T. Colin, D. Bresch, J.P. Boissel, E. Grenier, and J.P. Flandrois, *A pharmacologically based multiscale mathematical model of angiogenesis and its use in investigating the efficacy of a new cancer treatment strategy*, J. Theor. Biol., 260(4), 545–562, 2009.

[3] V. Capasso and D. Morale, *Stochastic modelling of tumour-induced angiogenesis*, J. Math. Biol., 58, 219–233, 2009.

[4] R.P. Fedkiw, T. Aslam, B. Merriman, and S. Osher, *A non-oscillatory Eulerian approach to interfaces in multimaterial flows (the ghost fluid method)*, J. Comp. Phys., 152, 457–492, 1999.

[5] F. Mac Gabhann and A.S. Popel, *Dimerization of vegf receptors and implications for signal transduction: A computational study*, Biophys. Chem., 128(2C3), 125–139, 2007.

[6] J.L. Gevertz and S. Torquato, *Modeling the effects of vasculature evolution on early brain tumor growth*, J. Theor. Biol., 243, 517–531, 2006.

[7] D. Hanahan and J. Folkman, *Patterns and emerging mechanisms of the angiogenic switch during tumorigenesis*, Cell, 86, 353–364, 1996.

[8] M.J. Holmes and B.D. Sleeman, *A mathematical model of tumor angiogenesis incorporating cellular traction and viscoelastic effects*, J. Theor. Biol., 202, 95–112, 2000.

[9] P.I. Imoukhuede and A.S. Popel, *Quantification and cell-to-cell variation of vascular endothelial growth factor receptors*, Exp. Cell Res., 317(7), 955 – 965, 2011.

[10] T. Jackson and X. Zheng, *A cell-based model of endothelial cell migration, proliferation and maturation during corneal angiogenesis*, Bull. Math. Biol., 72, 830–868, 2010.

[11] H.A. Levine, S. Pamuk, B.D. Sleeman, and M. Nilsen-Hamilton, *Mathematical modeling of capillary formation and development in tumor angiogenesis: Penetration into the stroma*, Bull. Math. Biol., 63, 801–863, 2001.

[12] F. Li and X. Zheng, *Singularity analysis of a reaction-diffusion equation with a solution-dependent dirac delta source*, Appl. Math. Lett., 25, 2179–2183, 2012.

[13] F. Mac Gabhann, J.W. Ji, and A.S. Popel, *Computational model of vascular endothelial growth factor spatial distribution in muscle and pro-angiogenic cell therapy*, PLoS Comput. Biol., 2(9), e127, 2006.

[14] F. Mac Gabhann, J.W. Ji, and A.S. Popel, *VEGF gradients, receptor activation, and sprout guidance in resting and exercising skeletal muscle*, J. Appl. Physiol., 102, 722–734, 2007.

[15] F. Mac Gabhann and A.S. Popel, *Model of competitive binding of vascular endothelial growth factor and placental growth factor to VEGF receptors on endothelial cells*, Am. J. Physiol. Heart Circ. Physiol., 286(1), H153–164, 2004.

[16] P. Macklin, S. McDougall, A. Anderson, M. Chaplain, V. Cristini, and J. Lowengrub, *Multiscale modelling and nonlinear simulation of vascular tumour growth*, J. Math. Biol., 58, 765–798, 2009.

[17] I.V. Maly, S.H. Wiley, and D.A. Lauffenburger, *Self-organization of polarized cell signaling via autocrine circuits: computational model analysis*, Biophys. J., 86(1), 10–22, 2004.

[18] D. Manoussaki, *A mechanochemical model of angiogenesis and vasculogenesis*, ESAIM:M2AN, 37, 581–599, 2003.

[19] F. Milde, M. Bergdorf, and P. Koumoutsakos, *A hybrid model for three-dimensional simulations of sprouting angiogenesis*, Biophys. J., 95, 3146–3160, 2008.

[20] C.V. Pao and W.H. Ruan, *Positive solutions of quasilinear parabolic systems with nonlinear boundary conditions*, J. Math. Anal. Appl., 333(1), 472–499, 2007.

[21] M.J. Plank and B.D. Sleeman, *Lattice and non-lattice models of tumour angiogenesis*, Bull. Math. Biol., 66, 1785–1819, 2004.

[22] M.J. Plank, B.D. Sleeman, and P.F. Jones, *A mathematical model of tumour angiogenesis, regulated by vascular endothelial growth factor and the angiopoietins*, J. Theor. Biol., 229, 435–454, 2004.

[23] P. Quittner and P. Souplet, *Superlinear parabolic problems. Blow-up, global existence and steady states*, Birkhäuser Advanced Texts: Basler Lehrbücher Birkhäuser Verlag, Basel, 2007.

[24] R.C. Schugart, A. Friedman, R. Zhao, and C.K. Sen, *Wound angiogenesis as a function of tissue oxygen tension: A mathematical model*, PNAS, 105, 2628–2633, 2008.

[25] G. Serini, D. Ambrosi, E. Giraudo, A. Gamba, L. Preziosi, and F. Bussolino, *Modeling the early stages of vascular network assembly*, EMBO, 22, 1771–1779, 2003.

[26] M.M. Sholley, G.P. Ferguson, H.R. Seibel, J.L. Montour, and J.D. Wilson, *Mechanisms of neovascularization. Vascular sprouting can occur without proliferation of endothelial cells*, Lab. Invest., 51, 624–634, 1984.

[27] S. Sun, M.F. Wheeler, M. Obeyesekere, and C. Patrick, *A deterministic model of growth factor-induced angiogenesis*, Bull. Math. Biol., 67, 313–337, 2005.

[28] S. Sun, M.F. Wheeler, M. Obeyesekere, and C. Patrick Jr, *Multiscale angiogenesis modeling using mixed finite element methods*, Multiscale Model. Simul., 4, 1137, 2005.

[29] R.D.M. Travasso, E. Corvera Poir, M. Castro, J.C. Rodrguez-Manzaneque, and A. Hernndez-Machado, *Tumor angiogenesis and vascular patterning: A mathematical model*, PLoS ONE, 6(5), e19989, 05 2011.

[30] C. Xue, A. Friedman, and C.K. Sen, *A mathematical model of ischemic cutaneous wounds*, PNAS, 106(39), 16782–16787, 2009.

[31] X. Zheng, Y. Kim, E.-B. Lin, and L. Rakesh, *A conservative and variation preserving finite volume method for non-overlapping meshes of reaction and diffusion in angiogenesis*, J. Comput. Appl. Math., 275, 183–196, 2015.

[32] X. Zheng, G.Y. Koh, and T. Jackson, *A continuous model of angiogenesis: initiation, extension, and maturation of new blood vessels modulated by vascular endothelial growth factor, angiopoietins, platelet-derived growth factor-B, and pericytes*, Discrete Contin. Dyn. Syst. Ser. B, 18, 1109–1154, 2013.

[33] X. Zheng, S. Wise, and V. Cristini, *Nonlinear simulation of tumor necrosis, neovascularization and tissue invasion via an adaptive finte-element/level-set method*, Bull. Math. Biol., 67, 211–259, 2005.